mRNA vaccine-elicited antibodies to SARS-CoV-2 and circulating variants

Zijun Wang[1,*], Fabian Schmidt[2,*], Yiska Weisblum[2,*], Frauke Muecksch[2,*], Christopher O. Barnes[3,*], Shlomo Finkin[1,*], Dennis Schaefer-Babajew[1,*], Melissa Cipolla[1*], Christian Gaebler[1*], Jenna A. Lieberman[4,*], Zhi Yang[3], Morgan E. Abernathy[3], Kathryn E. Huey-Tubman[3], Arlene Hurley[5], Martina Turroja[1], Kamille A. West[6], Kristie Gordon[1], Katrina G. Millard[1], Victor Ramos[1], Justin Da Silva[2], Jianliang Xu[4], Robert A. Colbert[7], Roshni Patel[1], Juan Dizon[1], Cecille Unson-O'Brien[1], Irina Shimeliovich[1], Anna Gazumyan[1], Marina Caskey[1], Pamela J. Bjorkman[3,#], Rafael Casellas[4,8,#], Theodora Hatziioannou[2,#], Paul D. Bieniasz[2,9,#], Michel C. Nussenzweig[1,9,#]

[1]Laboratory of Molecular Immunology, The Rockefeller University, New York, NY 10065, USA.

[2]Laboratory of Retrovirology, The Rockefeller University, New York, NY 10065, USA.

[3] Division of Biology and Biological Engineering, California Institute of Technology, Pasadena, CA, USA.

[4]Lymphocyte Nuclear Biology, National Institute of Arthritis and Musculoskeletal and Skin Diseases, National Institutes of Health, Bethesda, MD 20892.

[5]Hospital Program Direction, The Rockefeller University, New York, NY 10065, USA.

[6]Department of Transfusion Medicine, National Institutes of Health Clinical Center, Bethesda, MD 20892.

23 [7]Pediatric Translational Research Branch and Office of the Clinical Director, National Institute
24 of Arthritis and Musculoskeletal and Skin Diseases, National Institutes of Health, Bethesda, MD
25 20892.
26 [8]The NIH Regulome Project, National Institutes of Health, Bethesda, MD 20892.
27 [9] Howard Hughes Medical Institute
28
29 [*]Equal contribution
30
31 [#]Send correspondence to Paul Bieniasz: pbieniasz@rockefeller.edu; Pamela Bjorkman:
32 bjorkman@caltech.edu; Rafael Casellas: rafael.casellas@nih,gov; Theodora Hatziioannou:
33 thatziio@rockefeller.edu; Michel C. Nussenzweig: nussen@rockefeller.edu
34

To date severe acute respiratory syndrome coronavirus-2 (SARS-CoV-2) has infected nearly 100 million individuals resulting in over two million deaths. Many vaccines are being deployed to prevent coronavirus disease-2019 (COVID-19) including two novel mRNA-based vaccines[1,2]. These vaccines elicit neutralizing antibodies and appear to be safe and effective, but the precise nature of the elicited antibodies is not known[3-5]. Here we report on the antibody and memory B cell responses in a cohort of 20 volunteers who received either the Moderna (mRNA-1273) or Pfizer-BioNTech (BNT162b2) vaccines. Consistent with prior reports, 8 weeks after the second vaccine injection volunteers showed high levels of IgM, and IgG anti-SARS-CoV-2 spike protein (S), receptor binding domain (RBD) binding titers[3,5]. Moreover, the plasma neutralizing activity, and the relative numbers of RBD-specific memory B cells were equivalent to individuals who recovered from natural infection[6,7]. However, activity against SARS-CoV-2 variants encoding E484K or N501Y or the K417N:E484K:N501Y combination was reduced by a small but significant margin. Consistent with these findings, vaccine-elicited monoclonal antibodies (mAbs) potently neutralize SARS-CoV-2, targeting a number of different RBD epitopes epitopes in common with mAbs isolated from infected donors. Structural analyses of mAbs complexed with S trimer suggest that vaccine- and virus-encoded S adopts similar conformations to induce equivalent anti-RBD antibodies. However, neutralization by 14 of the 17 most potent mAbs tested was reduced or abolished by either K417N, or E484K, or N501Y mutations. Notably, the same mutations were selected when recombinant vesicular stomatitis virus (rVSV)/SARS-CoV-2 S was cultured in the presence of the vaccine elicited mAbs. Taken together the results suggest that the monoclonal antibodies in clinical use

57 **should be tested against newly arising variants, and that mRNA vaccines may need to be**

58 **updated periodically to avoid potential loss of clinical efficacy.**

59 Between 19 October 2020 and 15 January 2021, 20 volunteers who received two doses of the
60 Moderna (n=14) or Pfizer-BioNTech mRNA (n=6) vaccines were recruited for blood donation
61 and analyzed. Ages of the analyzed volunteers ranged from 29-69 years (median 43); 12
62 (60%) were male and 8 (40%) female. 16 participants identified as Caucasian, 2 as Hispanic, and
63 1 as African American or Asian, respectively. The time from the second vaccination to sample
64 collection varied between 3-14 weeks with an average of 8 weeks. None of the volunteers had a
65 history of prior SARS-CoV-2 infection and none experienced serious adverse events after
66 vaccination (Extended Data Table 1).
67
68 **Vaccinee plasma binding and neutralizing activity against SARS-CoV-2**
69 Plasma IgM and IgG anti-SARS-CoV-2 S and RBD were measured by enzyme-linked
70 immunosorbent assay (ELISA)[6,7]. All individuals tested showed reactivity to S and RBD that
71 was significantly higher compared to pre-COVID-19 historic controls (Extended Data Fig 1). As
72 might be expected anti-S and -RBD IgG levels were higher than IgM or IgA. Moreover, there
73 was greater variability in the anti-RBD than the anti-S response but the two were positively
74 correlated (Extended Data Fig 1).
75
76 Plasma neutralizing activity was determined using HIV-1 pseudotyped with SARS-CoV-2 S
77 protein[6-8]. In agreement with previous reports, there was a broad range of plasma neutralizing
78 activity 3-14 weeks after the second vaccine dose that was similar to that elicited by natural
79 infection in a convalescent cohort after 1.3 months, and greater than the activity at 6.2 months
80 after infection (Fig. 1a, Extended Data Table 1). There was no significant difference in
81 neutralizing activity between the Moderna and Pfizer-BioNTech vaccines (Fig. 1b). As

82 expected, plasma neutralizing activity was directly correlated to anti-S and -RBD binding titers
83 in ELISAs[6,7] (Fig. 1c, d, and Extended Data Fig. 2a-d). Finally, RBD and S binding, and
84 neutralizing activities were directly correlated to the time between the first vaccine dose and
85 blood donation with significantly reduced levels in all 3 measurements with time (Fig. 1e-g, and
86 Extended Data Fig. 2e-h)[9].
87
88 To determine whether plasma from vaccinated individuals can neutralize circulating SARS-CoV-
89 2 variants of concern and mutants that arise *in vitro* under antibody pressure [10,11], we tested
90 vaccinee plasma against a panel of 10 mutant pseudotype viruses including recently reported
91 N501Y (B1.1.7 variant), K417N, E484K and the combination of these 3 RBD mutations
92 (501Y.V2 variant)[12-17]. Vaccinee plasma was significantly less effective in neutralizing the HIV-
93 1 virus pseudotyped with certain SARS-CoV-2 mutant S proteins (Fig. 1h and i and Extended
94 Data Fig. 2j). Among the volunteer plasmas tested there was an 1 to 3, 1.3 to 2.5, and 1.1 to 3
95 fold decrease in neutralizing activity against E484K, N501Y and the K417N:E484K:N501Y
96 combination respectively ($p= 0.0033$, $p=0.0002$, and $p<0.0001$, respectively, Fig. 1h and i). We
97 conclude that the plasma neutralizing activity elicited by mRNA vaccination is variably but
98 significantly less effective against particular RBD mutants in the tested panel.
99
100 **Vaccine-elicited SARS-CoV-2 RBD-specific monoclonal antibodies**
101 Although circulating antibodies derived from plasma cells wane over time, long-lived immune
102 memory can persist in expanded clones of memory B cells[6]. We used flow cytometry to
103 enumerate the circulating SARS-CoV-2 RBD-specific memory B cells elicited by mRNA
104 immunization[6,7] (Fig. 2a, Extended Data Fig. 3a and b). Notably, the percentage of RBD-binding

105 memory B cells in vaccinees was significantly greater than in naturally infected individuals
106 assayed after 1.3 months, but similar to the same individuals assayed after 6.2 months (Fig. 2b).
107 The percentage of RBD-binding memory B cells in vaccinees was not correlated to the time after
108 vaccination (Extended Data Fig. 3c). Thus, mRNA vaccination elicits a robust SARS-CoV-2
109 RBD-specific B cell memory response that resembles natural infection.
110
111 To examine the nature of the antibodies produced by memory B cells in response to vaccination,
112 we obtained 1,409 paired antibody heavy and light chains from RBD binding single B cells from
113 14 individuals (n=10 Moderna and n=4 Pfizer-BioNTech vaccinees) (Extended Data Table 2).
114 Expanded clones of cells comprised 4-50% of the overall RBD binding memory B cell
115 compartment (Fig. 2c and d, and Extended Data Fig. 3d). Similar to natural infection, IGVH 3-
116 53, and 3-30 and some IGVL genes were significantly over-represented in the RBD-binding
117 memory B cell compartment of vaccinated individuals (Fig. 2e, Extended Data Fig. 4a). In
118 addition, antibodies that share the same combination of IGHV and IGLV genes in vaccinees
119 comprised 39% of all the clonal sequences (Extended Data Fig. 4b) and 59% when combined
120 with naturally infected individuals[6,7] (Fig. 2f), and some of these antibodies were nearly identical
121 (Extended Data Table 2 and 3). The number of V gene nucleotide mutations in vaccinees is
122 greater than in naturally infected individuals assayed after 1.3 months, but lower than that in the
123 same individuals assayed after 6.2 months (Fig. 2g and Extended Data Fig. 5a). The length of the
124 IgH CDR3 was similar in both natural infected individuals and vaccinees and hydrophobicity
125 was below average[18] (Fig. 2h and Extended Data Fig. 5a and b). Thus, the IgG memory response
126 is similar in individuals receiving the Pfizer-BioNTech and Moderna vaccines and both are rich
127 in recurrent and clonally expanded antibody sequences.

128

129 Eighty-four representative antibodies from 4 individuals were expressed and tested for reactivity
130 to the RBD (Extended Data Table 4). The antibodies included: (1) 58 that were randomly
131 selected from those that appeared only once, and (2) 26 representatives of expanded clones. Of
132 the antibodies tested 99% (83 out of the 84) bound to RBD indicating that single cell sorting by
133 flow cytometry efficiently identified B cells producing anti-RBD antibodies (Extended Data Fig.
134 6a and b and Table 4). In anti-RBD ELISAs the mean half-maximal effective concentration
135 (EC_{50}) was higher than that observed in infected individuals after 6 months but not significantly
136 different from antibodies obtained 1.3 months after infection (Extended Data Fig. 6a, and Table
137 4 and [6,7]). To examine memory B cell antibodies for binding to circulating SARS-CoV-2 variants
138 and antibody resistant mutants we performed ELISA assays using mutant RBDs[10,13,19-22].
139 Twenty-two (26%) of the antibodies showed at least 5-fold decreased binding to at least one of
140 the mutant RBDs (Extended data Fig. 6c-l, and Table 4).

141

142 SARS-CoV-2 S pseudotyped viruses were used to measure the neutralizing activity of all 84
143 antibodies[6-8] (Fig. 3a, Extended Data Table 4). Consistent with the plasma neutralization results,
144 the geometric mean neutralization half-maximal inhibitory concentration of the vaccinee
145 antibodies (IC_{50}=151 ng/ml) was not significantly different to antibody collections obtained from
146 naturally infected individuals 1.3 or 6.2 months after infection (Fig. 3a and [6,7]).

147

148 To examine the neutralizing breadth of the monoclonal antibodies and begin to map their target
149 epitopes we tested the 17 most potent antibodies (Extended data Table 5), 8 of which carried
150 IgHV3-53, against a panel of 12 SARS-CoV-2 variants: A475V is resistant to class 1 antibodies

151 (structurally defined as described[20]); E484K and Q493R are resistant to class 2
152 antibodies[6,7,10,11,20,21,23,24]; while R346S, N439K, and N440K are resistant to class 3
153 antibodies[6,7,10,11,20,24]. Additionally, K417N, Y453F, S477R, N501Y, D614G, and R683G
154 represent circulating variants some of which have been associated with rapidly increasing case
155 numbers[12,13,24-27]. Based on their neutralizing activity against the variants, all but 3 of the
156 antibodies were provisionally assigned to a defined antibody class or a combination (Fig. 3b). As
157 seen in natural infection, a majority of the antibodies tested (9/17) were at least ten-fold less
158 effective against pseudotyped viruses carrying the E484K mutation[6,10,20]. In addition, 5 of the
159 antibodies were less potent against K417N and 4 against N501Y by ten-fold or more (Fig. 3b).
160
161 To determine whether antibody-imposed selection pressure could also drive the emergence of
162 resistance mutations *in vitro,* we cultured an rVSV/SARS-CoV-2 recombinant virus in the
163 presence of each of 18 neutralizing monoclonal antibodies. All of the tested antibodies selected
164 for RBD mutations. Moreover, in all cases the selected mutations corresponded to residues in the
165 binding sites of their presumptive antibody class (Fig. 3b and c). For example, antibody 627,
166 which was assigned to class 2 based on sensitivity to E484K mutation, selected for the
167 emergence of the E484K mutation *in vitro* (Fig 3c). Notably, 6 of the antibodies selected for
168 K417N E or T, 5 selected for E484K and 3 selected for N501Y, T or H, which coincide with
169 mutations present in the circulating B1.1.17, 501Y.V2 and B1.1.28/501.V3 variants that have
170 been associated with rapidly increasing case numbers in particular locales[12,15,17,28].
171
172 **Cryo-EM mapping of antibody epitopes**

173 To further characterize antibody epitopes and mechanisms of neutralization, we characterized
174 seven complexes between mAb Fab fragments and the prefusion, stabilized ectodomain trimer of
175 SARS-CoV-2 S glycoprotein[29] using single-particle cryo-EM (Fig. 4 and Extended Data Table
176 6). Overall resolutions ranged from 5-8 Å and coordinates from S trimer and representative Fab
177 crystal structures were fit by rigid body docking into the cryo-EM density maps to provide a
178 general assessment of antibody footprints/RBD epitopes. Fab-S complexes exhibited multiple
179 RBD-binding orientations recognizing either 'up'/'down' (Fig. 4a-j) or solely 'up' (Fig. 4k-n)
180 RBD conformations, consistent with structurally defined antibody classes from natural infection
181 (Fig. 4o)[20]. The majority of mAbs characterized (6 of 7) recognized epitopes that included RBD
182 residues involved in ACE2 recognition, suggesting a neutralization mechanism that directly
183 blocks ACE2-RBD interactions. Additionally, structurally defined antibody epitopes were
184 consistent with RBD positions that were selected in rVSV/SARS-CoV-2 recombinant virus
185 outgrowth experiments, including residues K417, N439/N440, E484, and N501 (Fig. 3c and Fig.
186 4f-j,m,n). Taken together, these data suggest that functionally similar antibodies are raised during
187 vaccination and natural infection, and that the RBDs of spike trimers translated from the mRNA
188 delivered by vaccination adopt a similar distribution of 'up'/'down' conformations as observed
189 on SARS-CoV-2 virions.
190

191 **Discussion**

192 The mRNA-based SARS-CoV-2 vaccines are safe and effective and being deployed globally to
193 prevent infection and disease. The vaccines elicit antibody responses against the RBD, the major
194 target of neutralizing antibodies[30-35], in a manner that resembles natural infection. Notably, the
195 neutralizing antibodies produced by mRNA vaccination target the same epitopes as natural

196 infection. The data is consistent with SARS-CoV-2 spike trimers translated from the injected
197 RNA adopting the range of conformations available to spikes on the surfaces of virions.
198 Moreover, different individuals immunized with either the Moderna (mRNA-1273) or Pfizer-
199 BioNTech (BNT162b2) vaccines produce closely related and nearly identical antibodies.
200
201 Human neutralizing monoclonal antibodies to the SARS-CoV-2 RBD can be categorized as
202 belonging to 4 different classes based on their target regions on the RBD[20]. Class 1 and 2
203 antibodies are among the most potent and also the most abundant antibodies[6,7,30,31,34]. These
204 antibodies target epitopes that overlap or are closely associated with RBD residues K417, E484
205 and N501. They are frequently sensitive to mutation in these residues and select for K417N,
206 E484K and N501Y mutations in both yeast and VSV expressing SARS-CoV-2 S proteins[10,13,24].
207 To avert selection and escape, antibody therapies should be composed of combinations of
208 antibodies that target non-overlapping epitopes[7,10,11,24,36-38].
209
210 A number of circulating SARS-CoV-2 variants that have been associated with rapidly increasing
211 case numbers and have particular prevalence in the UK (B1.1.7/501Y.V1), South Africa
212 (501Y.V2) and Brazil (B1.1.28/501.V3)[12,15,17,28,39]. Our experiments indicate that these variants,
213 and potentially others that carry K417N/T, E484K and N501Y mutations, can reduce the
214 neutralization potency of vaccinee plasma. The comparatively modest effects of the mutations on
215 viral sensitivity to plasma reflects the polyclonal nature of the neutralizing antibodies in vaccinee
216 plasma. Nevertheless, emergence of these particular variants is consistent with the dominance of
217 the class 1 and 2 antibody response in infected or vaccinated individuals and raises the
218 possibility that they emerged in response to immune selection in individuals with non-sterilizing

219 immunity. What the long-term effect of accumulation of mutations on the SARS-CoV-2
220 pandemic will be is not known, but the common cold coronavirus HCoV-229E evolves antigenic
221 variants that are comparatively resistant to the older sera but remain sensitive to
222 contemporaneous sera[40]. Thus, it is possible that these mutations and others that emerge in
223 individuals with suboptimal or waning immunity will erode the effectiveness of natural and
224 vaccine elicited immunity. The data suggests that SARS-CoV-2 vaccines may need to be updated
225 and immunity monitored in order to compensate for viral evolution.
226

227 **Figure Legends**

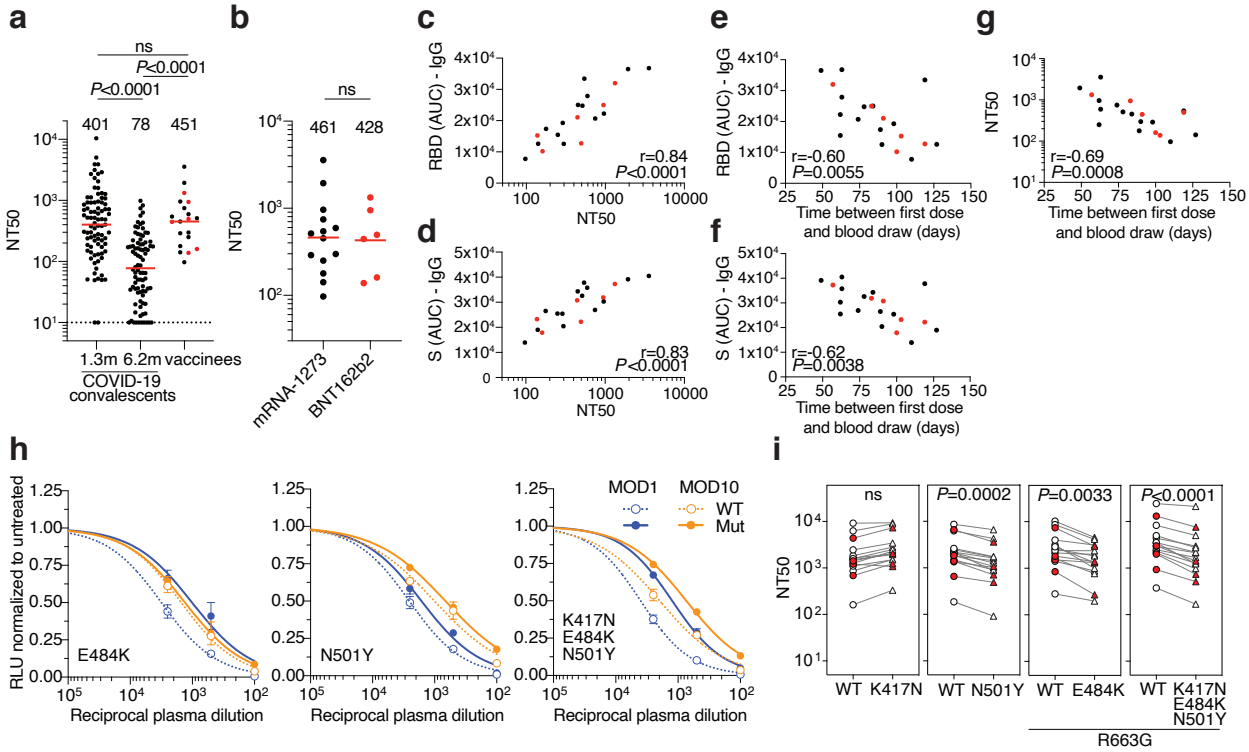

228

229 **Fig. 1. Plasma neutralizing activity. a,** SARS-CoV-2 pseudovirus neutralization assay. NT_{50}

230 values for COVID-19 convalescent plasma measured at 1.3 months[7] and 6.2 months[6] as well as

231 plasma from mRNA-vaccinees. NT_{50} values lower than 10 were plotted at 10. Mean of 2

232 independent experiments. Red bars and indicated values represent geometric mean NT_{50} values.

233 Statistical significance was determined using the two-tailed Mann-Whitney U-test. **b**, NT_{50}

234 values for Moderna (black) and Pfizer-BioNTech (red) vaccine recipients. Red bars and

235 indicated values represent geometric mean NT_{50} values. Statistical significance was determined

236 using the two-tailed Mann-Whitney U-test. **c**, Anti-RBD IgG AUC (Y axis) plotted against NT_{50}

237 (X axis) r=0.84, p<0.0001. **d,** Anti-S IgG AUC (Y axis) plotted against NT_{50} (X axis) r=0.83,

238 p<0.0001. **e**, Anti-RBD IgG AUC (Y axis) plotted against time between first dose and blood

239 draw (X axis) r=-0.60 p=0.0055. **f**, Anti-S IgG AUC (Y axis) plotted against time between first

240 dose and blood draw (X axis) r=-0.62 p=0.0038. **g**, NT_{50} (Y axis) plotted against time between
241 first dose and blood draw (X axis) r=-0.69 p=0.0008. The r and p values for correlations in **c-g**
242 were determined by two-tailed Spearman correlation. Moderna vaccinees are in black and Pfizer-
243 BioNTech in red. **h.** Examples of neutralization assays, comparing the sensitivity of pseudotyped
244 viruses with WT and RBD mutant SARS-CoV-2 S proteins to vaccinee plasma. **i,** NT50 values
245 for vaccinee plasma (n=15) neutralization of pseudotyped viruses with WT and the indicated
246 RBD-mutant SARS-CoV-2 S proteins. Statistical significance was determined using one tailed t-
247 test. All experiments were performed a minimum of 2 times. Pfizer-BioNTech vaccinees in red.
248

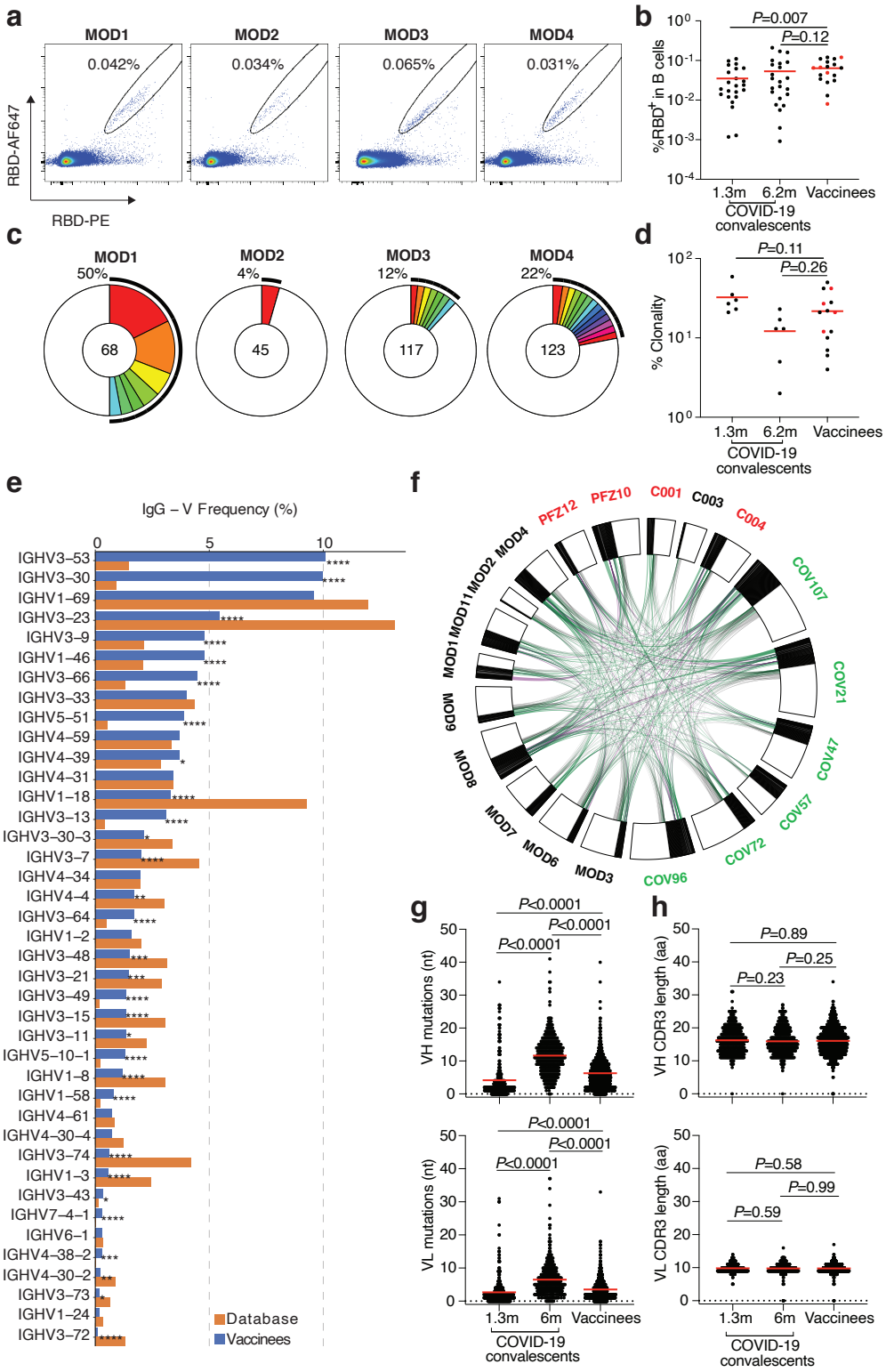
a
MOD1
MOD2
MOD3
MOD4
0.042%
0.034%
0.065%
0.031%
RBD-AF647
RBD-PE
b
P=0.007
P=0.12
%RBD+ in B cells
1.3m
6.2m
Vaccinees
COVID-19 convalescents
c
MOD1
MOD2
MOD3
MOD4
50%
4%
12%
22%
68
45
117
123
d
P=0.11
P=0.26
% Clonality
1.3m
6.2m
Vaccinees
COVID-19 convalescents
e
IgG – V Frequency (%)
IGHV3–53
IGHV3–30
IGHV1–69
IGHV3–23
IGHV3–9
IGHV1–46
IGHV3–66
IGHV3–33
IGHV5–51
IGHV4–59
IGHV4–39
IGHV4–31
IGHV1–18
IGHV3–13
IGHV3–30–3
IGHV3–7
IGHV4–34
IGHV4–4
IGHV3–64
IGHV1–2
IGHV3–48
IGHV3–21
IGHV3–49
IGHV3–15
IGHV3–11
IGHV5–10–1
IGHV1–8
IGHV1–58
IGHV4–61
IGHV4–30–4
IGHV3–74
IGHV1–3
IGHV3–43
IGHV7–4–1
IGHV6–1
IGHV4–38–2
IGHV4–30–2
IGHV3–73
IGHV1–24
IGHV3–72
Database
Vaccinees
f
PFZ12
PFZ10
C001
C003
C004
COV107
COV21
COV47
COV57
COV72
COV96
MOD3
MOD6
MOD7
MOD8
MOD9
MOD1
MOD11
MOD2
MOD4
g
P<0.0001
P<0.0001
P<0.0001
VH mutations (nt)
P<0.0001
P<0.0001
P<0.0001
VL mutations (nt)
1.3m
6m
Vaccinees
COVID-19 convalescents
h
P=0.89
P=0.25
P=0.23
VH CDR3 length (aa)
P=0.58
P=0.99
P=0.59
VL CDR3 length (aa)
1.3m
6m
Vaccinees
COVID-19 convalescents

249

250 **Fig. 2. Memory B cell antibodies. a**, Representative flow cytometry plots showing dual
251 AlexaFluor-647-RBD and PE-RBD binding B cells for 4 vaccinees. **b,** as in **a,** dot plot
252 summarizes the percentage of RBD binding B cells in 19 vaccinees, in comparison to a cohort of
253 infected individuals assays 1.3 and 6.2 months after infection[6,7]. Individuals who received the
254 Moderna vaccine are shown in black and Pfizer-BioNTech vaccine recipients in red. Red
255 horizontal bars indicate mean values. Statistical significance was determined using two-tailed
256 Mann–Whitney U-tests. **c,** Pie charts show the distribution of antibody sequences from the 4
257 individuals in **a.** The number in the inner circle indicates the number of sequences analyzed. Pie
258 slice size is proportional to the number of clonally related sequences. The black outline indicates
259 the frequency of clonally expanded sequences. **d,** as in **c,** graph shows relative clonality among
260 14 vaccinees assayed, individuals who received the Moderna vaccine are shown in black and
261 Pfizer-BioNTech vaccine recipients in red. Red horizontal bars indicate mean values. Statistical
262 significance was determined using two-tailed Mann–Whitney U-tests. **e,** Graph shows relative
263 abundance of human IGVH genes Sequence Read Archive accession SRP010970 (orange), and
264 vaccinees (blue). A two-sided binomial test was used to compare the frequency distributions,
265 significant differences are denoted with stars (* $p < 0.05$, ** $p < 0.01$, *** $p < 0.001$, **** = $p <$
266 0.0001). **f,** Clonal relationships between sequences from 14 vaccinated individuals (Moderna in
267 black, Pfizer-BioNTech in red Extended Data Table 2) and naturally infected individuals (in
268 green, from[6,7]). Interconnecting lines indicate the relationship between antibodies that share V
269 and J gene segment sequences at both IGH and IGL. Purple, green and grey lines connect related
270 clones, clones and singles, and singles to each other, respectively. **g,** Number of somatic
271 nucleotide mutations in the IGVH (top) and IGVL (bottom) in vaccinee antibodies (Extended
272 Data Table 2) compared to natural infection obtained 1.3 or 6.2 months after infection[6,7].

273 Statistical significance was determined using the two-tailed Mann–Whitney U-tests and red

274 horizontal bars indicate mean values. **h,** as in **g,** but for CDR3 length.

275

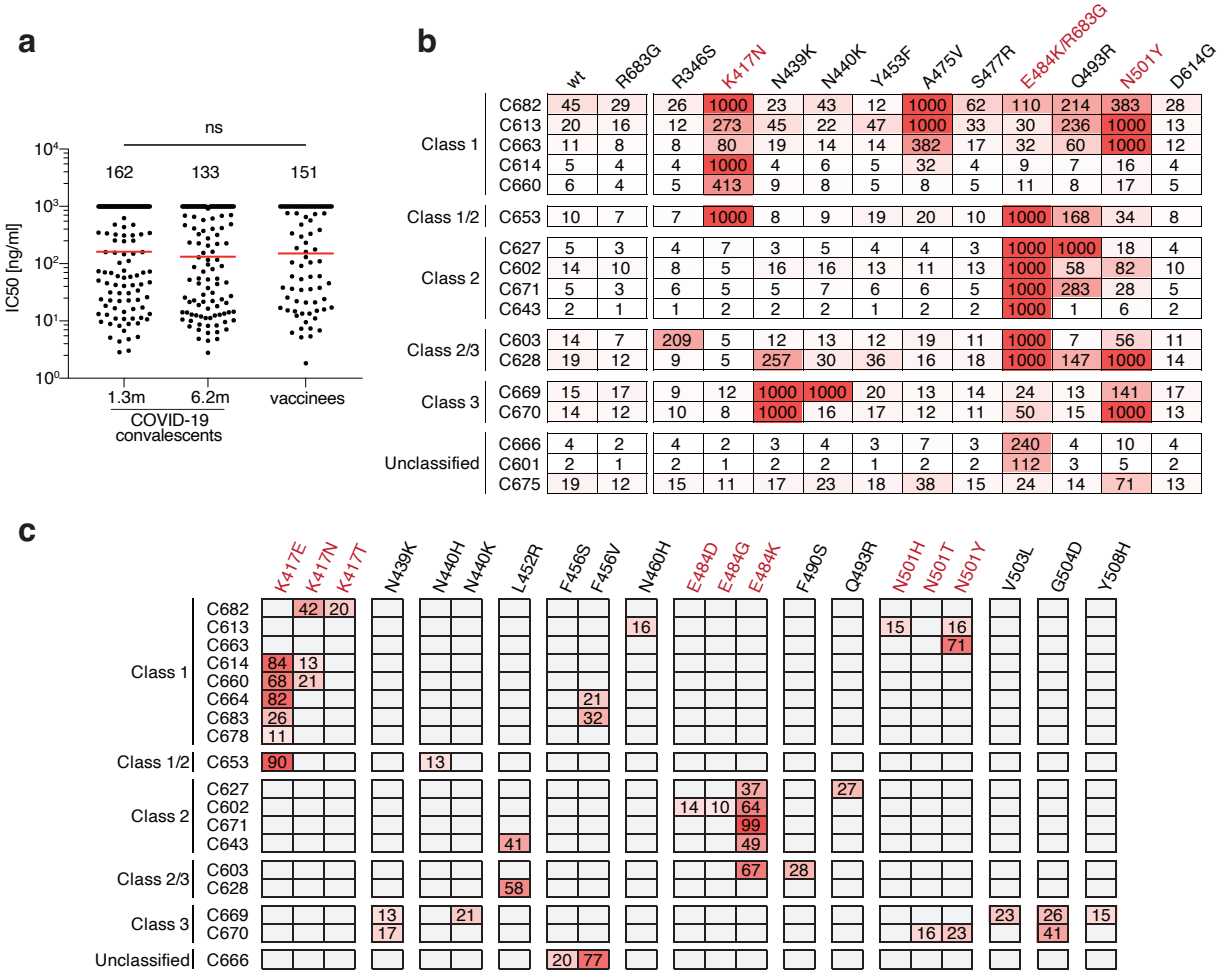

Fig. 3: Anti-SARS-CoV-2 RBD monoclonal antibody neutralizing activity. a, SARS-CoV-2 pseudovirus neutralization assay. IC_{50} values for antibodies cloned from COVID-19 convalescent patients measured at 1.3 and 6.2 months[6,7] as well as antibodies cloned from mRNA-vaccinees. Antibodies with IC_{50} values above 1000 ng/ml were plotted at 1000 ng/ml. Mean of 2 independent experiments. Red bars and indicated values represent geometric mean IC_{50} values in ng/ml. Statistical significance was determined using the two-tailed Mann-Whitney U-test. **b,** IC_{50} values for 17 selected mAbs for neutralization of wild type and the indicated mutant SARS-CoV-2 pseudoviruses. Color gradient indicates IC_{50} values ranging from 0 (white)

285 to 1000 ng/ml (red). **c**, Antibody selection pressure can drive emergence of S variants in cell
286 culture; the percentage of sequence reads encoding the indicated RBD mutations after a single
287 passage of rVSV/SARS-CoV-2 in the presence of the indicated antibodies is tabulated. Color
288 gradient indicates percentage of sequence reads bearing the indicated mutation ranging from 0
289 (white) to 100 (red). Positions for which no sequence read was detected are shown in grey.
290 K417N, E484K/R683G and N501 are highlighted in b and c as they constitute important
291 circulating variants.
292

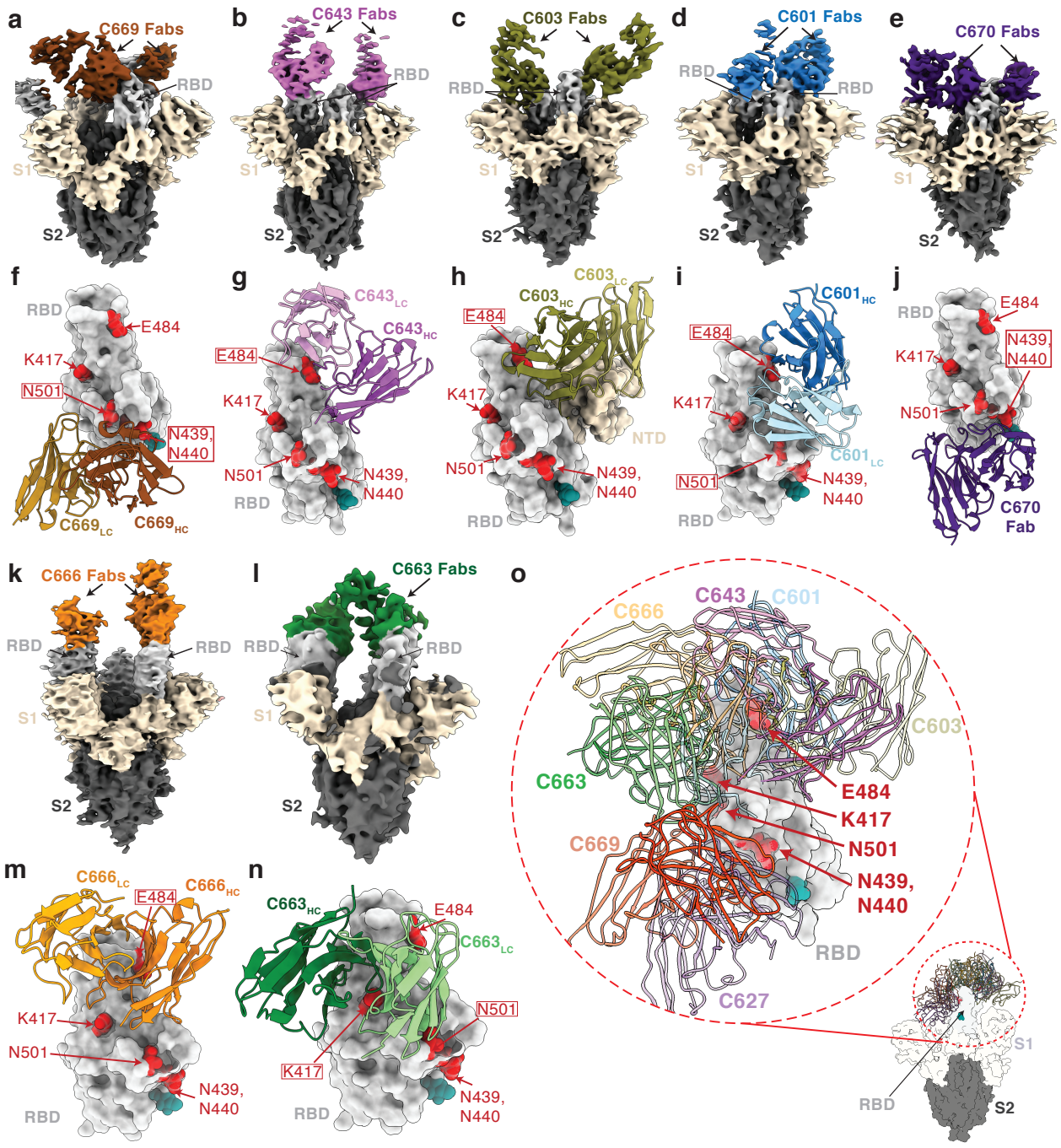

Fig. 4. Cryo-EM reconstructions of Fab-S complexes. Cryo-EM densities for Fab-S complexes (**a-e**; **k-l**) and close-up views of antibody footprints on RBDs (**f-j**; **m-n**) are shown for neutralizing mAbs. As expected due to Fab inter-domain flexibility, cryo-EM densities (**a-e**; **k-l**) were weak for the Fab C_H-C_L domains. Models of antibody footprints on RBDs (**f-j**; **m-n**) are

298 presented as Fab V_H-V_L domains (cartoon) complexed with the RBD (surface). To generate
299 models, coordinates of stabilized S trimer (PDB 6XKL) and representative Fab fragments (PDB
300 6XCA or 7K8P) with CDR3 loops removed were fit by rigid body docking into the cryo-EM
301 density maps. **a,f,** C669; **b,g,** C643; **c,h,** C603; **d,i,** C601; **e,j,** C670; **k,m,** C666; and **l,n,** C663.
302 RBD residues K417, N439, N440, E484, and N501 are highlighted as red surfaces. The N343
303 glycan is shown as a teal sphere. **o,** Composite model illustrating targeted epitopes of RBD-
304 specific neutralizing mAbs (shown as V_H-V_L domains in colors from panels **a-l**) elicited from
305 mRNA vaccines.
306

307 **Methods**

308 **Data reporting**

309 No statistical methods were used to predetermine sample size. The experiments were not
310 randomized and the investigators were not blinded to allocation during experiments and outcome
311 assessment.

312

313 **Study participants**.

314 To isolate and characterize anti-SARS-CoV-2 RBD antibodies from vaccinees, a cohort
315 of 20 individuals that participated in either the Moderna or Pfizer-BioNTech phase 3 vaccine
316 clinical trials and did not report prior history of SARS-CoV-2 infection was recruited at the NIH
317 Blood Center and the Rockefeller University Hospital for blood donation. Eligible participants
318 included adults, at least 18 years of age with no known heart, lung, kidney disease or bleeding
319 disorders, no history of HIV-1 or malaria infection. All participants were asymptomatic at the
320 time of the study visit and had received a complete 2 dose regimen of either mRNA vaccine.
321 Informed consent was obtained from all participants and the study was conducted in accordance
322 with Good Clinical Practice. The study visits and blood draws were reviewed and approved
323 under the National Institutes of Health's Federalwide Assurance (FWA00005897), in accordance
324 with Federal regulations 45 CFR 46 and 21 CFR 5 by the NIH Intramural Research Program IRB
325 committee (IRB# 99CC0168, Collection and Distribution of Blood Components from Healthy
326 Donors for In Vitro Research Use) and by the Institutional Review Board of the Rockefeller
327 University (IRB# DRO-1006, Peripheral Blood of Coronavirus Survivors to Identify Virus-
328 Neutralizing Antibodies). For detailed participant characteristics see Extended Data Table SI 1.

329

330 **Blood samples processing and storage.**

331 Samples collected at NIH were drawn from participants at the study visit and processed within
332 24 hours. Briefly, whole blood samples were subjected to Ficoll gradient centrifugation after 1:1
333 dilution in PBS. Plasma and PBMC samples were obtained through phase separation of plasma
334 layer and Buffy coat phase, respectively. PBMCs were further prepared through centrifugation,
335 red blood cells lysis and washing steps, and stored in CellBanker cell freezing media
336 (Amsbio). All samples were aliquoted and stored at - 80 °C and shipped on dry ice. Prior to
337 experiments, aliquots of plasma samples were heat-inactivated (56°C for 1 hour) and then stored
338 at 4°C. Peripheral Blood Mononuclear Cells (PBMCs) obtained from samples collected at
339 Rockefeller University were purified as previously reported[6,7] by gradient centrifugation and
340 stored in liquid nitrogen in the presence of FCS and DMSO. Heparinized plasma samples were
341 aliquoted and stored at -20°C or less. Prior to experiments, aliquots of plasma samples were heat-
342 inactivated (56°C for 1 hour) and then stored at 4°C.

343

344

345 **ELISAs**

346 ELISAs[41,42] to evaluate antibodies binding to SARS-CoV-2 S (BioHub), RBD and additional
347 mutated RBDs were performed by coating of high-binding 96-half-well plates (Corning 3690)
348 with 50 µl per well of a 1µg/ml protein solution in PBS overnight at 4 °C. Plates were washed 6
349 times with washing buffer (1× PBS with 0.05% Tween-20 (Sigma-Aldrich)) and incubated with
350 170 µl per well blocking buffer (1× PBS with 2% BSA and 0.05% Tween-20 (Sigma)) for 1 h at
351 room temperature. Immediately after blocking, monoclonal antibodies or plasma samples were
352 added in PBS and incubated for 1 h at room temperature. Plasma samples were assayed at a

353 1:66.6 (RU samples) or a 1:33.3 (NIH samples) starting dilution and 7 additional threefold serial
354 dilutions. Monoclonal antibodies were tested at 10 µg/ml starting concentration and 10 additional
355 fourfold serial dilutions. Plates were washed 6 times with washing buffer and then incubated
356 with anti-human IgG, IgM or IgA secondary antibody conjugated to horseradish peroxidase
357 (HRP) (Jackson Immuno Research 109-036-088 109-035-129 and Sigma A0295) in blocking
358 buffer at a 1:5,000 dilution (IgM and IgG) or 1:3,000 dilution (IgA). Plates were developed by
359 addition of the HRP substrate, TMB (ThermoFisher) for 10 min (plasma samples) or 4 minutes
360 (monoclonal antibodies), then the developing reaction was stopped by adding 50 µl 1 M H_2SO_4
361 and absorbance was measured at 450 nm with an ELISA microplate reader (FluoStar Omega,
362 BMG Labtech) with Omega and Omega MARS software for analysis. For plasma samples, a
363 positive control (plasma from participant COV72[6,7], diluted 66.6-fold and with seven additional
364 threefold serial dilutions in PBS) was added to every assay plate for validation. The average of
365 its signal was used for normalization of all of the other values on the same plate with Excel
366 software before calculating the area under the curve using Prism V8.4 (GraphPad). For
367 monoclonal antibodies, the EC50 was determined using four-parameter nonlinear regression
368 (GraphPad Prism V8.4).
369
370 **Expression of RBD proteins**
371 Mammalian expression vectors encoding the RBDs of SARS-CoV-2 (GenBank MN985325.1; S
372 protein residues 319-539) and eight additional mutant RBD proteins (E484K, Q493R, R346S,
373 N493K, N440K, V367F, A475V, S477N and V483A) with an N-terminal human IL-2 or Mu
374 phosphatase signal peptide were previously described[21].
375

376 **Cells and viruses**

377 293T/ACE2.cl22 and HT1080/ACE2.cl14 cells[8] were cultured in Dulbecco's Modified Eagle
378 Medium (DMEM) supplemented with 10% fetal bovine serum (FBS) at 37°C and 5% CO_2. Cells
379 were periodically tested for contamination with mycoplasma or retroviruses.
380 rVSV/SARS-CoV-2/GFP chimeric virus stocks were generated by infecting 293T/ACE2.cl22
381 cells. Supernatant was harvested 1 day post infection (dpi), cleared of cellular debris, and stored
382 at -80°C. A plaque purified variant designated rVSV/SARS-CoV-2/GFP_{2E1} that encodes
383 D215G/R683G substitutions was used in these studies[8].
384

385 **Selection and analysis of antibody escape mutations**

386 For the selection of monoclonal antibody-resistant spike variants, a rVSV/SARS-CoV-2/GFP_{2E1}
387 (for details see[8]) population containing 10^6 infectious units was incubated with of monoclonal
388 antibodies (10 μg/ml passage 10-40 μg/ml for 1 hr at 37 °C. Then, the virus-antibody mixtures
389 were incubated with 5×10^5 293T/ACE2cl.22 cells in 6-well plates. At 1 day post infection media
390 was replaced with fresh media containing the equivalent concentrations of antibodies.
391 Supernatant was harvested 2 days after infection and 150 μl of the cleared supernatant was used
392 to infect cells for passage 2, while 150 μl was subjected to RNA extraction and sequencing.
393 For identification of putative antibody resistance mutations, RNA was extracted using
394 NucleoSpin 96 Virus Core Kit (Macherey-Nagel). The RNA was reversed transcribed using the
395 SuperScript VILO cDNA Synthesis Kit (Thermo Fisher Scientific). KOD Xtreme Hot Start DNA
396 Polymerase (Millipore Sigma) was used for amplification of cDNA using primers flanking the S-
397 encoding sequence. The PCR products were purified and sequenced as previously described[6,10].
398 Breifly, tagmentation reactions were performed using 1ul diluted cDNA, 0.25 μl Nextera TDE1

399 Tagment DNA enzyme (catalog no. 15027865), and 1.25 μl TD Tagment DNA buffer (catalog
400 no. 15027866; Illumina). Next, the DNA was ligated to unique i5/i7 barcoded primer
401 combinations using the Illumina Nextera XT Index Kit v2 and KAPA HiFi HotStart ReadyMix
402 (2X; KAPA Biosystems) and purified using AmPure Beads XP (Agencourt), after which the
403 samples were pooled into one library and subjected to paired-end sequencing using Illumina
404 MiSeq Nano 300 V2 cycle kits (Illumina) at a concentration of 12pM.
405 For analysis of the sequencing data, the raw paired-end reads were pre-processed to remove trim
406 adapter sequences and to remove low-quality reads (Phred quality score < 20) using BBDuk.
407 Reads were mapped to the rVSV/SARS-CoV-2/GFP sequence using Geneious Prime (Version
408 2020.1.2). Mutations were annotated using Geneious Prime, with a P-value cutoff of 10^{-6}.
409

410 **SARS-CoV-2 pseudotyped reporter virus**

411 A panel of plasmids expressing RBD-mutant SAR-CoV-2 spike proteins in the context of
412 pSARS-CoV-2-$S_{\Delta 19}$ have been described previously[10]. Additional substitutions were introduced
413 using either PCR primer-mediated mutagenesis or with synthetic gene fragments (IDT) followed
414 by Gibson assembly. The mutants E484K and KEN (K417N+E484K+N501Y) were constructed
415 in the context of a pSARS-CoV-2-$S_{\Delta 19}$ variant with a mutation in the furin cleavage site
416 (R683G). The NT50s and IC50 of these pseudotypes were compared to a wildtype SARS-CoV-2
417 (NC_045512) spike sequence carrying R683G in the subsequent analyses, as appropriate.
418 Generation of SARS-CoV-2 pseudotyped HIV-1 particles was performed as previously
419 described[7]. Briefly, 293T cells were transfected with pNL4-3ΔEnv-nanoluc and pSARS-CoV-2-
420 $S_{\Delta 19}$ and pseudotyped virus stocks were harvested 48 hours after transfection, filtered and stored
421 at -80°C.

422

423 **SARS-CoV-2 pseudotype neutralization assays**

424 Plasma or monoclonal antibodies from vaccine recipients were four-fold or five-fold serially
425 diluted and then incubated with SARS-CoV-2 pseudotyped HIV-1 reporter virus for 1 h at 37 °C.
426 The antibody and pseudeotype virus mixture was added to $293T_{Ace2}$ cells[7] (for comparisons of
427 plasma from COVID-19-convalescents and vaccine recipients) or HT1080ACE2.cl14 cells[8] (for
428 analysis of spike mutants with vaccine recipient plasma or monoclonal antibodies). After 48 h
429 cells were washed with PBS and lysed with Luciferase Cell Culture Lysis 5× reagent (Promega)
430 and Nanoluc Luciferase activity in lysates was measured using the Nano-Glo Luciferase Assay
431 System (Promega) with the Glomax Navigator (Promega). The relative luminescence units were
432 normalized to those derived from cells infected with SARS-CoV-2 pseudotyped virus in the
433 absence of plasma or monoclonal antibodies. The half-maximal neutralization titers for plasma
434 (NT_{50}) or half-maximal and 90% inhibitory concentrations for monoclonal antibodies (IC_{50} and
435 IC_{90}, respectively) were determined using four-parameter nonlinear regression (least squares
436 regression method without weighting; constraints: top=1, bottom=0) (GraphPad Prism).

437

438 **Biotinylation of viral protein for use in flow cytometry**

439 Purified and Avi-tagged SARS-CoV-2 RBD was biotinylated using the Biotin-Protein Ligase-
440 BIRA kit according to manufacturer's instructions (Avidity) as described before[7]. Ovalbumin
441 (Sigma, A5503-1G) was biotinylated using the EZ-Link Sulfo-NHS-LC-Biotinylation kit
442 according to the manufacturer's instructions (Thermo Scientific). Biotinylated ovalbumin was
443 conjugated to streptavidin-BV711 (BD biosciences, 563262) and RBD to streptavidin-PE (BD
444 Biosciences, 554061) and streptavidin-AF647 (Biolegend, 405237)[7].

445

446 **Flow cytometry and single cell sorting**

447 Single-cell sorting by flow cytometry was performed as described previously[7]. Briefly,
448 peripheral blood mononuclear cells were enriched for B cells by negative selection using a pan-
449 B-cell isolation kit according to the manufacturer's instructions (Miltenyi Biotec, 130-101-638).
450 The enriched B cells were incubated in FACS buffer (1× PBS, 2% FCS, 1 mM EDTA) with the
451 following anti-human antibodies (all at 1:200 dilution): anti-CD20-PECy7 (BD Biosciences,
452 335793), anti-CD3-APC-eFluro 780 (Invitrogen, 47-0037-41), anti-CD8-APC-eFluor 780
453 (Invitrogen, 47-0086-42), anti-CD16-APC-eFluor 780 (Invitrogen, 47-0168-41), anti-CD14-
454 APC-eFluor 780 (Invitrogen, 47-0149-42), as well as Zombie NIR (BioLegend, 423105) and
455 fluorophore-labelled RBD and ovalbumin (Ova) for 30 min on ice. Single
456 CD3−CD8−CD14−CD16−CD20+Ova−RBD-PE+RBD-AF647+ B cells were sorted into
457 individual wells of 96-well plates containing 4 µl of lysis buffer (0.5× PBS, 10 mM DTT, 3,000
458 units/ml RNasin Ribonuclease Inhibitors (Promega, N2615) per well using a FACS Aria III and
459 FACSDiva software (Becton Dickinson) for acquisition and FlowJo for analysis. The sorted cells
460 were frozen on dry ice, and then stored at −80 °C or immediately used for subsequent RNA
461 reverse transcription.

462

463 **Antibody sequencing, cloning and expression**

464 Antibodies were identified and sequenced as described previously[7]. In brief, RNA from single
465 cells was reverse-transcribed (SuperScript III Reverse Transcriptase, Invitrogen, 18080-044) and
466 the cDNA stored at −20 °C or used for subsequent amplification of the variable IGH, IGL and
467 IGK genes by nested PCR and Sanger sequencing. Sequence analysis was performed using

468 MacVector. Amplicons from the first PCR reaction were used as templates for sequence- and
469 ligation-independent cloning into antibody expression vectors. Recombinant monoclonal
470 antibodies and Fabs were produced and purified as previously described[7].
471
472 **Cryo-EM sample preparation**
473 Expression and purification of SARS-CoV-2 6P stabilized S trimers[29] was conducted as
474 previously described[43]. Purified Fab and S 6P trimer were incubated at a 1.1:1 molar ratio per
475 protomer on ice for 30 minutes prior to deposition on a freshly glow-discharged 300 mesh,
476 1.2/1.3 Quantifoil copper grid. Immediately before 3 µl of complex was applied to the grid,
477 fluorinated octyl-malotiside was added to the Fab-S complex to a final detergent concentration of
478 0.02% w/v, resulting in a final complex concentration of 3 mg/ml. Samples were vitrified in
479 100% liquid ethane using a Mark IV Vitrobot after blotting for 3 s with Whatman No. 1 filter
480 paper at 22˚C and 100% humidity.
481
482 **Cryo-EM data collection and processing**
483 Data collection and processing followed a similar workflow to what has been previously
484 described in detail[20]. Briefly, micrographs were collected on a Talos Arctica transmission
485 electron microscope (Thermo Fisher) operating at 200 kV for all Fab-S complexes. Data were
486 collected using SerialEM automated data collection software[44] and movies were recorded with a
487 K3 camera (Gatan). For all datasets, cryo-EM movies were patch motion corrected for beam-
488 induced motion including dose-weighting within cryoSPARC v2.15[45] after binning super
489 resolution movies. The non-dose-weighted images were used to estimate CTF parameters using
490 cryoSPARC implementation of the Patch CTF job. Particles were picked using Blob picker and

491 extracted 4x binned and 2D classified. Class averages corresponding to distinct views with
492 secondary structure features were chosen and ab initio models were generated. 3D classes that
493 showed features of a Fab-S complex were re-extracted, unbinned (0.869 Å/pixel) and
494 homogenously refined with C1 symmetry. Overall resolutions were reported based on gold
495 standard FSC calculations.
496

497 **Cryo-EM Structure Modeling and Refinement**

498 Coordinates for initial complexes were generated by docking individual chains from reference
499 structures into cryo-EM density using UCSF Chimera[46] (S trimer: PDB 6KXL, Fab: PDB 6XCA
500 or 7K8P after trimming CDR3 loops and converting to a polyalanine model). Models were then
501 refined into cryo-EM maps by rigid body and real space refinement in Phenix[47] If the resolution
502 allowed, partial CDR3 loops were built manually in Coot[48] and then refined using real-space
503 refinement in Phenix.
504

505 **Computational analyses of antibody sequences**

506 Antibody sequences were trimmed based on quality and annotated using Igblastn v.1.14. with
507 IMGT domain delineation system. Annotation was performed systematically using Change-O
508 toolkit v.0.4.540 [49]. Heavy and light chains derived from the same cell were paired, and
509 clonotypes were assigned based on their V and J genes using in-house R and Perl scripts
510 (Extended data Fig. 2). All scripts and the data used to process antibody sequences are publicly
511 available on GitHub (https://github.com/stratust/igpipeline).
512

513 The frequency distributions of human V genes in anti-SARS-CoV-2 antibodies from this study
514 was compared to 131,284,220 IgH and IgL sequences generated by [50] and downloaded from
515 cAb-Rep [51], a database of human shared BCR clonotypes available at https://cab-
516 rep.c2b2.columbia.edu/. Based on the 97 distinct V genes that make up the 4186 analyzed
517 sequences from Ig repertoire of the 14 participants present in this study, we selected the IgH and
518 IgL sequences from the database that are partially coded by the same V genes and counted them
519 according to the constant region. The frequencies shown in (Fig 2e and Extended Data Fig 3a**)**
520 are relative to the source and isotype analyzed. We used the two-sided binomial test to check
521 whether the number of sequences belonging to a specific IgHV or IgLV gene in the repertoire is
522 different according to the frequency of the same IgV gene in the database. Adjusted p-values
523 were calculated using the false discovery rate (FDR) correction. Significant differences are
524 denoted with stars.
525
526 Nucleotide somatic hypermutation and CDR3 length were determined using in-house R and Perl
527 scripts. For somatic hypermutations, IGHV and IGLV nucleotide sequences were aligned against
528 their closest germlines using Igblastn and the number of differences were considered nucleotide
529 mutations. The average mutations for V genes were calculated by dividing the sum of all
530 nucleotide mutations across all participants by the number of sequences used for the analysis. To
531 calculate the GRAVY scores of hydrophobicity[52] we used Guy H.R. Hydrophobicity scale based
532 on free energy of transfer (kcal/mole)[53] implemented by the R package Peptides (the
533 Comprehensive R Archive Network repository; https://journal.r-project.org/archive/2015/RJ-
534 2015-001/RJ-2015-001.pdf). We used 1409 heavy chain CDR3 amino acid sequences from this
535 study and 22,654,256 IGH CDR3 sequences from the public database of memory B cell receptor

536 sequences[54]. The two-tailed Wilcoxon nonparametric test was used to test whether there is a
537 difference in hydrophobicity distribution.
538
539 **Data availability statement:** Data are provided in SI Tables 1-8. The raw sequencing data and
540 computer scripts associated with Fig. 2 have been deposited at Github
541 (https://github.com/stratust/igpipeline). This study also uses data from "A Public Database of
542 Memory and Naive B-Cell Receptor Sequences" [54], PDB (6VYB and 6NB6) and from "High
543 frequency of shared clonotypes in human B cell receptor repertoires" [50]. Cryo-EM maps
544 associated with data reported in this manuscript will be deposited in the Electron Microscopy
545 Data Bank (EMDB: https://www.ebi.ac.uk/pdbe/emdb/).
546
547 **Data presentation**
548 Figures arranged in Adobe Illustrator 2020.
549
550 **Competing interests:** The Rockefeller University has filed a provisional patent application in
551 connection with this work on which Z.W. and M.C.N. are inventors (US patent 63/021,387).
552
553 **Code availability statement:** Computer code to process the antibody sequences is available at
554 GitHub (https://github.com/stratust/igpipeline).
555
556 **Acknowledgements:** We thank all study participants who devoted time to our research; Drs.
557 Barry Coller and Sarah Schlesinger, the Rockefeller University Hospital Clinical Research
558 Support Office and nursing staff; Charles M. Rice and all members of the M.C.N. laboratory for

helpful discussions and Maša Jankovic for laboratory support; and Dr. Jost Vielmetter and the Protein Expression Center in the Beckman Institute at Caltech for expression assistance. Electron microscopy was performed in the Caltech Beckman Institute Resource Center for Transmission Electron Microscopy and we thank Drs. Songye Chen and Andrey Malyutin for technical assistance. This work was supported by NIH grant P01-AI138398-S1 (M.C.N. and P.J.B.) and 2U19AI111825 (M.C.N.); the Caltech Merkin Institute for Translational Research and P50 AI150464-13 (P.J.B.), a George Mason University Fast Grant (P.J.B.); R37-AI64003 to P.D.B.; R01AI78788 to T.H.; We thank Dr. Jost Vielmetter and the Protein Expression Center in the Beckman Institute at Caltech for expression assistance C.O.B. is supported by the HHMI Hanna Gray and Burroughs Wellcome PDEP fellowships. C.G. was supported by the Robert S. Wennett Post-Doctoral Fellowship, in part by the National Center for Advancing Translational Sciences (National Institutes of Health Clinical and Translational Science Award program, grant UL1 TR001866), and by the Shapiro-Silverberg Fund for the Advancement of Translational Research. P.D.B. and M.C.N. are Howard Hughes Medical Institute Investigators.

Author Contributions:

P.D.B., P.J.B., R.C., T.H., M.C.N, Z.W., F.S., Y.W. F.M. C.O.B, S.F., D.S.B., M.Cipolla. conceived, designed and analyzed the experiments. M.Caskey, C.G., J.A. L, K.W. D.S.B. designed clinical protocols Z.W., F.S., Y.W. F.M. C.O.B, S.F., D.S.B., M.Cipolla, J.D.S. A.G. Z.Y., M.E.A., K.E.H. carried out experiments. C.G., M.Caskey, K.W. D., R.A.C., A.H., K.G.M. recruited participants and executed clinical protocols. I.S., R.P, J.D., J.X. and C.U.O. processed clinical samples. T.Y.O. and V.R. performed bioinformatic analysis. R.C. P.D.B., P.J.B., T.H., and M.C.N. wrote the manuscript with input from all co-authors.

582 **Extended Data Figures**

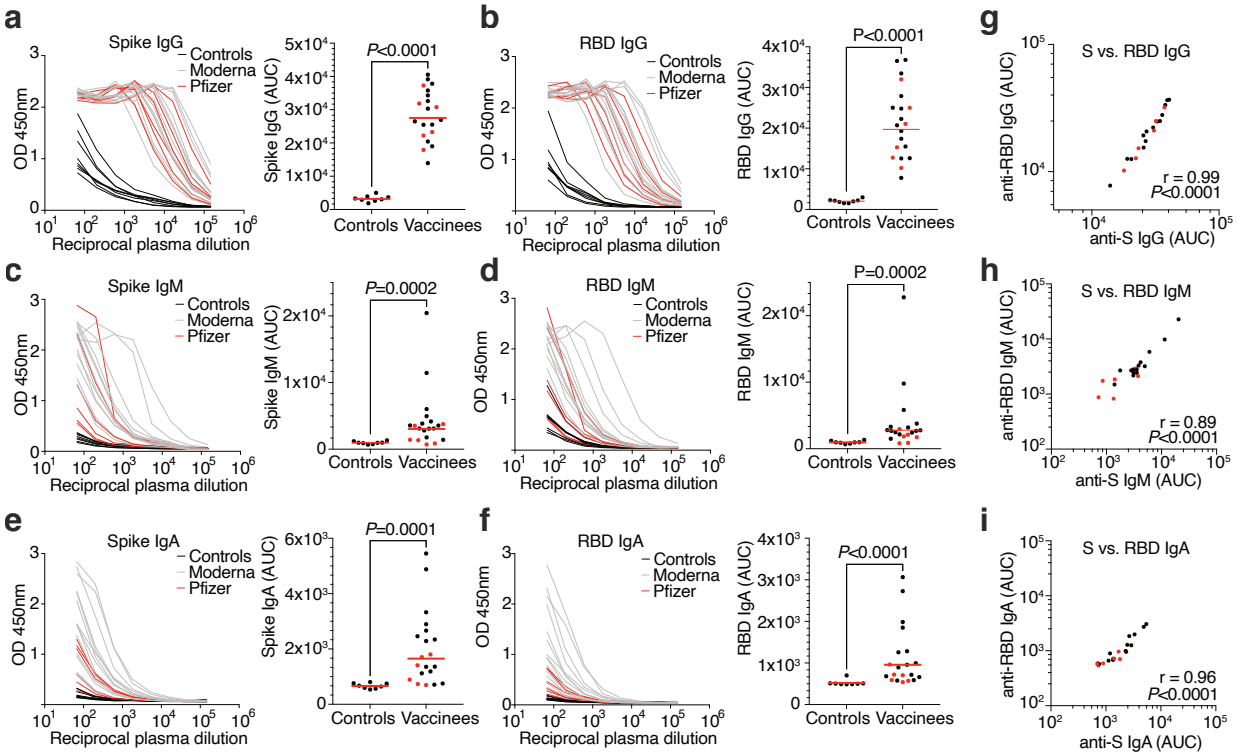

583

584 **Extended Data Fig. 1. Plasma antibodies against SARS-CoV-2.** **a**–**f**, Results of ELISAs
585 measuring plasma reactivity to S (**a**,**c**,**e**) and RBD protein (**b**,**d**,**f**) of 20 vaccinees (grey curves)
586 and 8 controls (black curves). **a**, Anti-S IgG. **b**, Anti-RBD IgG. **c**, Anti-S IgM. **d**, Anti-RBD
587 IgM. **e**, Anti-S IgA. **f**, Anti-RBD IgA. Left, optical density at 450 nm (OD 450 nm) for the
588 indicated reciprocal plasma dilutions. Right, normalized area under the curve (AUC) values for
589 the 8 controls and 20 vaccinees. Horizontal bars indicate geometric mean. Statistical significance
590 was determined using the two-tailed Mann–Whitney U-test. Average of two or more
591 experiments. **g-i,** Correlations of plasma antibodies measurements. **g,** Normalized AUC for IgG
592 anti-S plotted against normalized AUC for IgG anti-RBD. **h,** Normalized AUC for IgM anti-S
593 plotted against normalized AUC for IgM anti-RBD. **i,** Normalized AUC for IgA anti-S plotted
594 against normalized AUC for IgA anti-RBD. The *r* and *p* values in **g-i** were determined with the

595 two-tailed Spearman's correlation test. Moderna vaccinees are in black and Pfizer-BioNTech in

596 red.

597

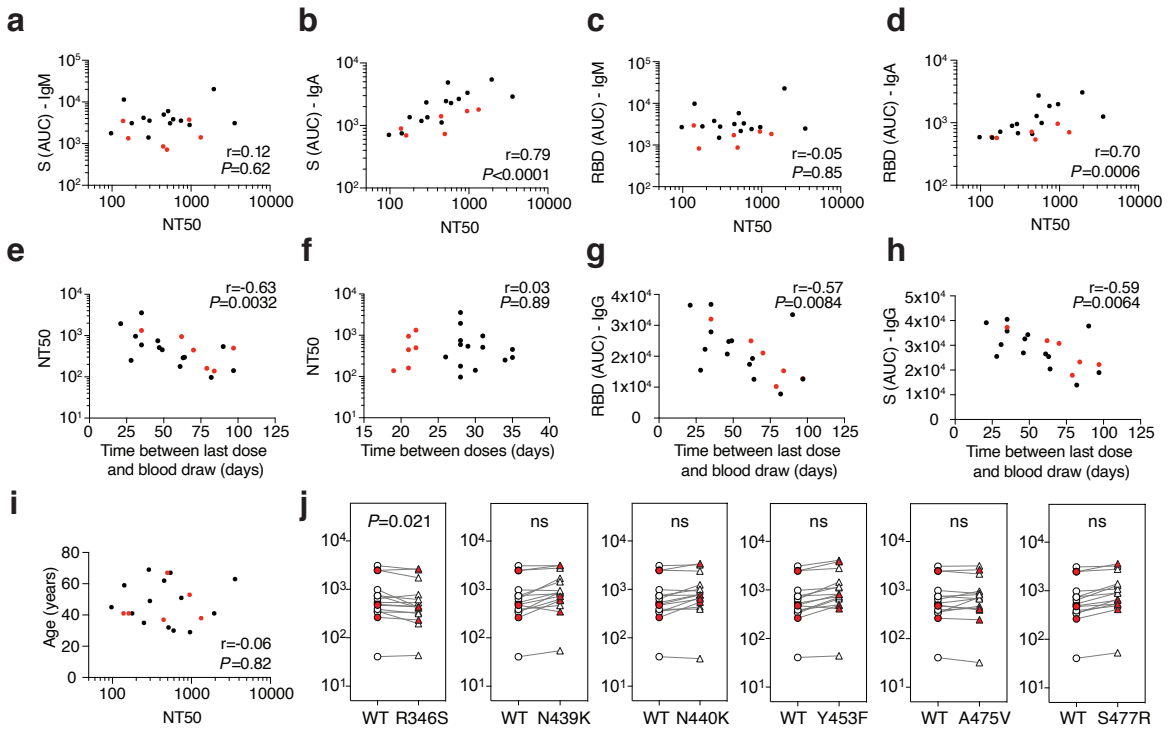

Extended Data Fig. 2: Plasma neutralizing activity. a, Anti-S IgM AUC (Y axis) plotted against NT_{50} (X axis) r=0.12, p<0.6179. **b,** Anti-S IgA AUC (Y axis) plotted against NT_{50} (X axis) r=0.79, p<0.0001. **c**, Anti-RBD IgM AUC (Y axis) plotted against NT50 (X axis) r=-0.05 p=0.8502. **d**, Anti-RBD IgA AUC (Y axis) plotted against NT50 (X axis) r=0.70 p=0.0006 **e**, NT_{50} (Y axis) plotted against time between last dose and blood draw (X axis) r=-0.63 p=0.0032. **f**, NT_{50} (Y axis) plotted against time between doses (X axis) r=0.03 p=0.8906. **g**, Anti-RBD IgG AUC (Y axis) plotted against time between last dose and blood draw (X axis) r=-0.57 p=0.0084. **h**, Anti-S IgG AUC (Y axis) plotted against time between last dose and blood draw (X axis) r=-0.59 p=0.0064. **i**, Age (Y axis) plotted against NT_{50} (X axis) r=-0.06 p=0.8150. The r and p values were determined by two-tailed Spearman's. Moderna vaccinees in black and Pfizer-BioNTech in red. **j**, NT50 values for vaccinee plasma (n=15) neutralization of pseudotyped

610 viruses with WT and the indicated RBD-mutant SARS-CoV-2 S proteins; p-values determined

611 using one tailed t-test.

612

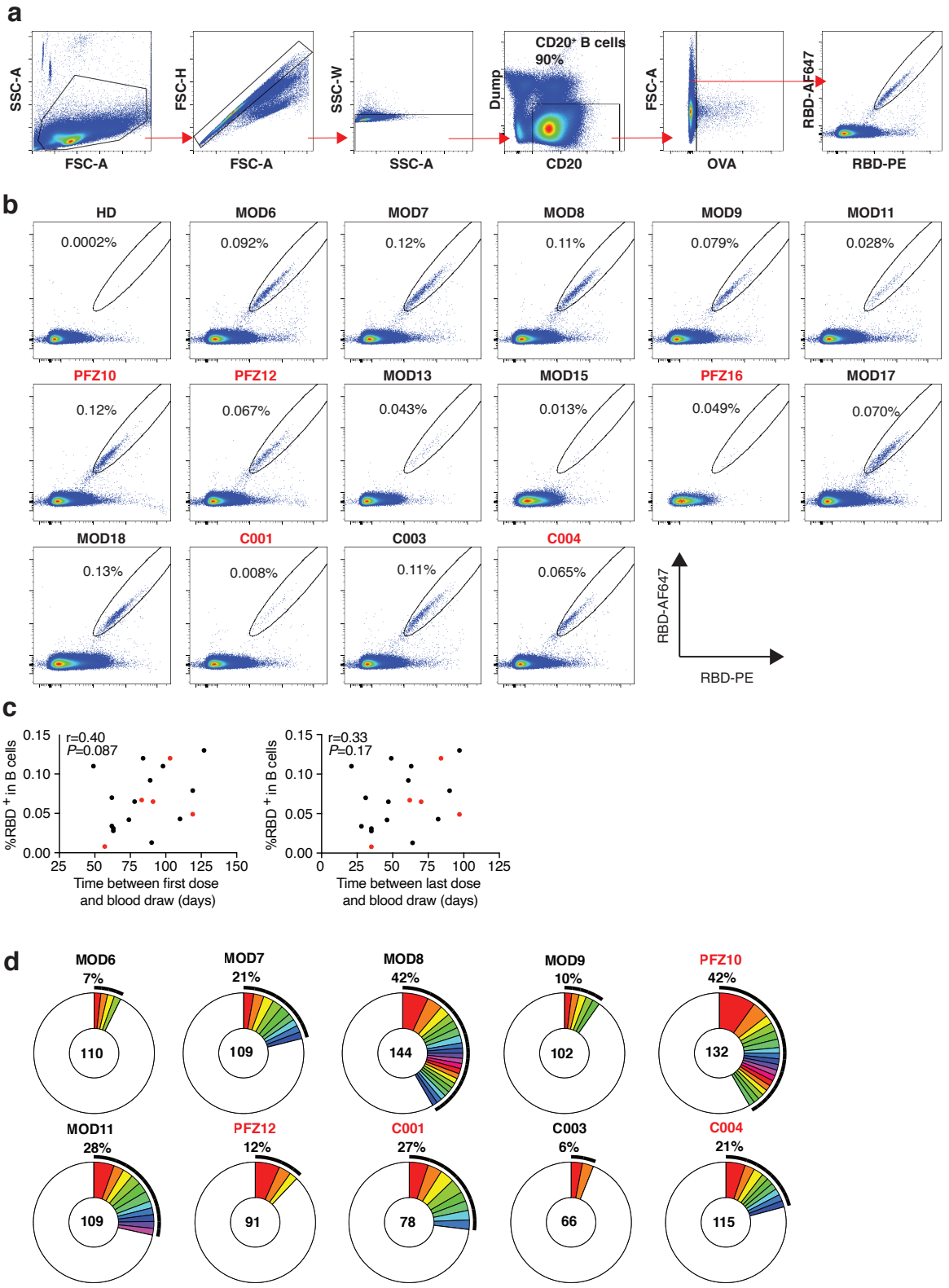
a
SSC-A
FSC-A
FSC-H
FSC-A
SSC-W
SSC-A
Dump
CD20⁺ B cells
90%
CD20
FSC-A
OVA
RBD-AF647
RBD-PE
b
HD
0.0002%
MOD6
0.092%
MOD7
0.12%
MOD8
0.11%
MOD9
0.079%
MOD11
0.028%
PFZ10
0.12%
PFZ12
0.067%
MOD13
0.043%
MOD15
0.013%
PFZ16
0.049%
MOD17
0.070%
MOD18
0.13%
C001
0.008%
C003
0.11%
C004
0.065%
RBD-AF647
RBD-PE
c
r=0.40
P=0.087
%RBD⁺ in B cells
Time between first dose
and blood draw (days)
r=0.33
P=0.17
%RBD⁺ in B cells
Time between last dose
and blood draw (days)
d
MOD6
7%
110
MOD7
21%
109
MOD8
42%
144
MOD9
10%
102
PFZ10
42%
132
MOD11
28%
109
PFZ12
12%
91
C001
27%
78
C003
6%
66
C004
21%
115

613

614 **Extended Data Fig. 3: Flow cytometry. a,** Gating strategy used for cell sorting. Gating was on
615 singlets that were CD20+ and CD3-CD8-CD16-OVA-. Sorted cells were RBD-PE+ and RBD-
616 AF647+. **b,** Flow cytometry showing the percentage of RBD-double positive memory B cells
617 from a pre-COVID-19 control (HD) and 15 vaccinees, who received the Moderna vaccine are
618 shown in black and Pfizer-BioNTech vaccine recipients are in red. **c**, the percentage of RBD-
619 binding memory B cells in vaccinees (Y axis) plotted against time between first dose and blood
620 draw (X axis) r=0.4028 p=0.0873 (left panel), and between last dose and blood draw (X axis)
621 r=0.3319 p=0.1651 (right panel). Moderna vaccinees in black and Pfizer-BioNTech in red. The r
622 and p values for correlations were determined by two-tailed Spearman's. **d,** Pie charts show the
623 distribution of antibody sequences from 10 individuals in **b.** The number in the inner circle
624 indicates the number of sequences analyzed. Pie slice size is proportional to the number of
625 clonally related sequences. The black outline indicates the frequency of clonally expanded
626 sequences. The r and p values for correlations in **c** were determined by the two-tailed Spearman
627 correlation test.
628

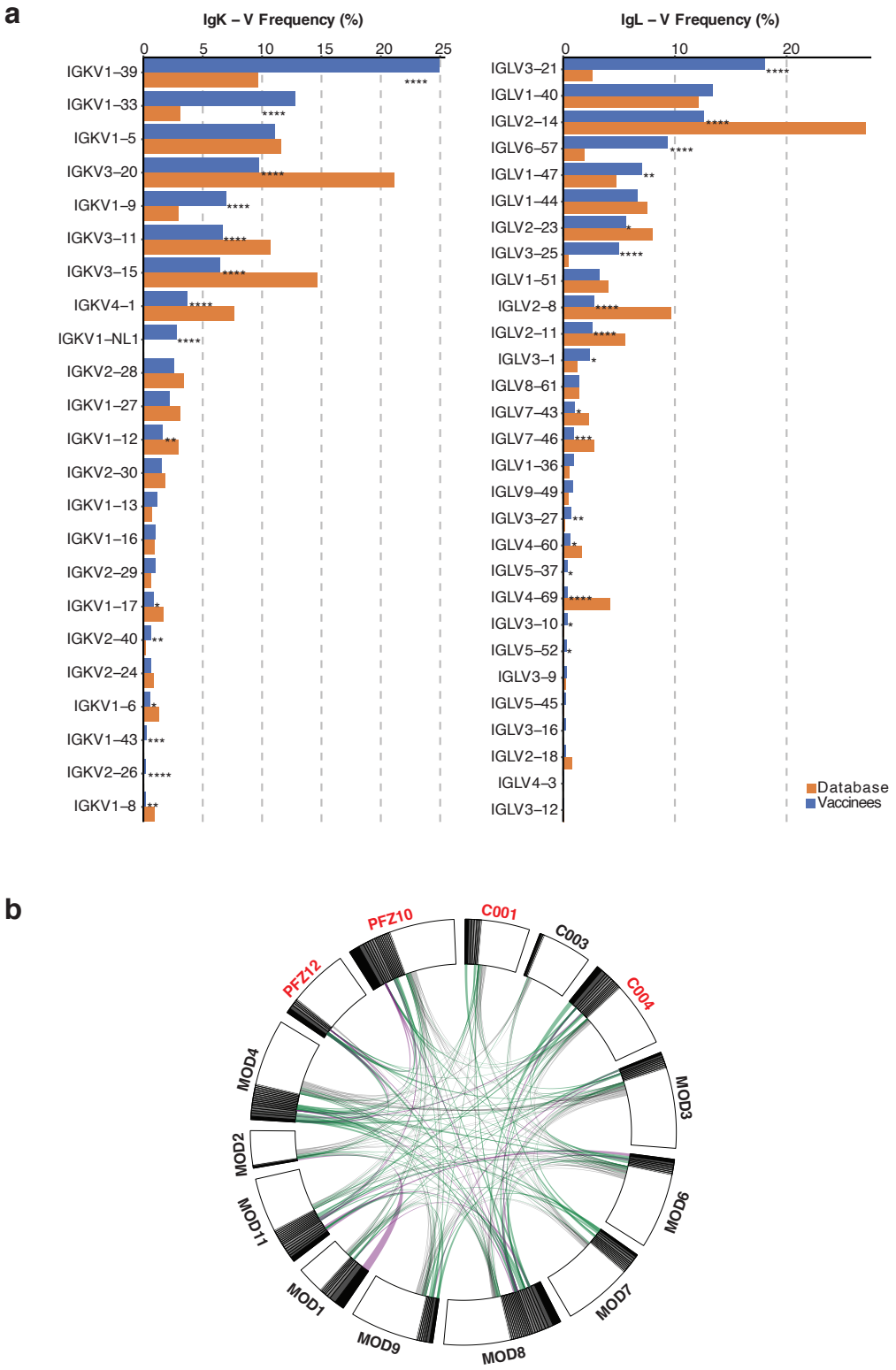

Extended Data Fig. 4: Frequency distributions of human VL genes.

631 Graph shows relative abundance of human IGVK (left) and IgVL (right) genes of Sequence Read
632 Archive accession SRP010970 (orange)[55], and vaccinees (blue). Two-sided binomial tests with
633 unequal variance were used to compare the frequency distributions., significant differences are
634 denoted with stars. (* $p < 0.05$, ** $p < 0.01$, *** $p < 0.001$, **** = $p < 0.0001$). **b.** Sequences
635 from 14 individuals (Extended Data Table 2) with clonal relationships depicted as in **c.**
636 Interconnecting lines indicate the relationship between antibodies that share V and J gene
637 segment sequences at both IGH and IGL. Purple, green and grey lines connect related clones,
638 clones and singles, and singles to each other, respectively.
639

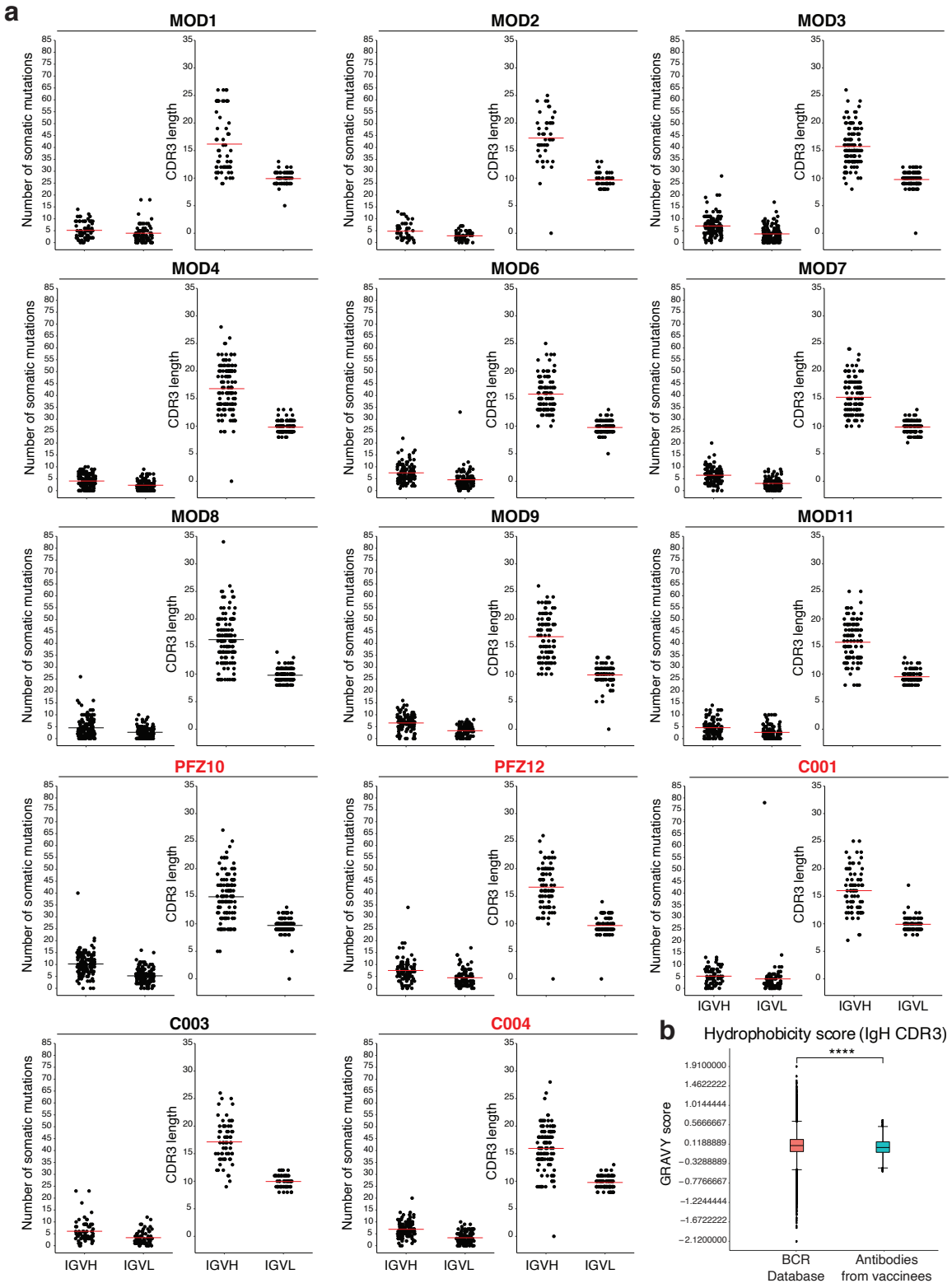
a
MOD1
MOD2
MOD3
MOD4
MOD6
MOD7
MOD8
MOD9
MOD11
PFZ10
PFZ12
C001
C003
C004
Number of somatic mutations
CDR3 length
IGVH
IGVL
b
Hydrophobicity score (IgH CDR3)
****
GRAVY score
BCR Database
Antibodies from vaccinees

640

641 **Extended Data Fig. 5: Antibody somatic hypermutation, and CDR3 length. a,** Number of
642 somatic nucleotide mutations in both the IGVH and IGVL in 14 participants (left). Individuals
643 who received the Moderna vaccine are shown in black and Pfizer-BioNTech vaccine recipients
644 in red. For each individual, the number of the amino acid length of the CDR3s at the IGVH and
645 IGVL is shown (right). The horizontal bars indicate the mean. The number of antibody
646 sequences (IGVH and IGVL) evaluated for each participant are n=68 (MOD1), n=45 (MOD2),
647 n=117 (MOD3), n=123 (MOD4), n=110 (MOD6), n=109 (MOD7), n=144 (MOD8), n=102
648 (MOD9), n=132 (PFZ10), n=109 (MOD11), n=91 (PFZ12), n=78 (C001), n=66 (C003), and
649 n=115 (C004). **b,** Distribution of the hydrophobicity GRAVY scores at the IGH CDR3 compared
650 to a public database (see Methods for statistical analysis). The box limits are at the lower and
651 upper quartiles, the center line indicates the median, the whiskers are 1.5× interquartile range and
652 the dots represent outliers. Statistical significance was determined using two-tailed Wilcoxon
653 matched-pairs signed rank test (n.s.=non-significant, **** = $p < 0.0001$).
654

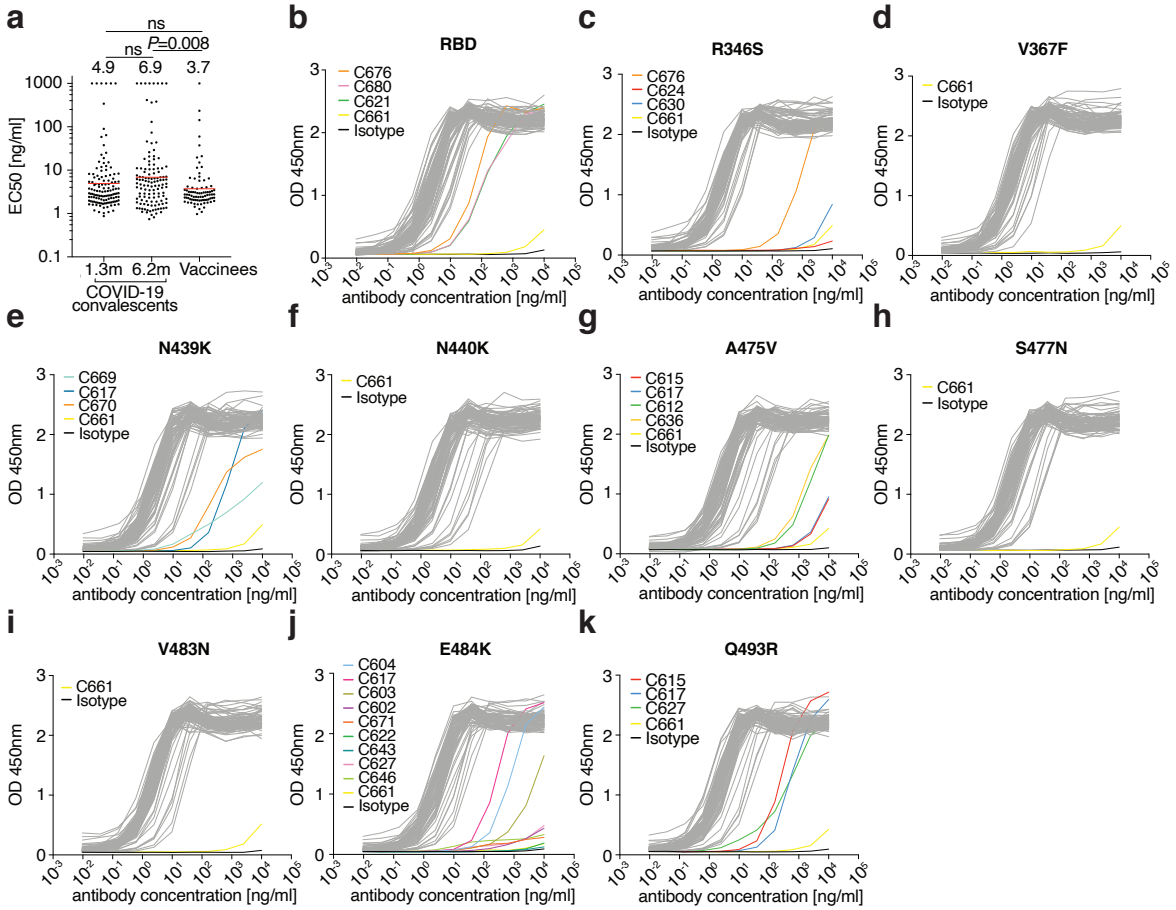

l

		wt	R346S	V367F	N439K	N440K	A475V	S477N	V483A	E484K	Q493R
Class 1	C682	2.4	2.2	2.6	3.6	3.5	35.0	3.3	2.8	3.7	4.1
	C613	2.0	1.9	1.8	3.3	2.5	126.1	2.4	2.3	2.2	4.9
	C663	1.9	1.8	1.7	2.7	2.5	12.6	2.3	2.0	2.4	2.2
	C614	1.4	1.6	1.6	2.0	1.9	2.5	1.8	1.9	1.6	1.8
	C660	2.0	2.0	2.1	2.3	2.7	2.5	2.1	2.2	2.4	2.2
Class 1/2	C653	2.1	2.1	2.1	2.5	2.6	2.2	2.1	2.3	4.0	3.1
Class 2	C627	1.6	1.6	1.8	2.0	2.0	2.1	1.9	1.8	1000	1000
	C602	2.0	1.8	1.9	2.1	2.2	2.2	2.1	3.1	1000	1.9
	C671	2.3	1.7	1.5	2.4	2.4	2.5	2.0	1.8	1000	2.5
	C643	2.1	2.2	2.3	2.0	2.2	1.7	1.8	2.5	1000	1.9
Class 2/3	C603	2.1	1.7	1.7	2.1	2.2	2.3	2.0	1.9	1000	1.9
	C628	2.7	1.9	2.0	4.3	3.2	3.1	2.4	2.4	10.0	3.2
Class 3	C669	2.3	2.1	2.2	950.6	291.8	2.1	2.1	2.2	2.4	2.2
	C670	2.9	2.1	2.3	210.7	2.8	3.0	2.6	2.4	3.3	3.3
Unclassified	C666	1.9	1.7	1.8	2.0	2.1	1.5	1.8	1.9	2.1	1.8
	C601	1.1	1.8	2.1	2.2	2.2	1.9	1.9	2.2	12.1	2.0
	C675	1.3	1.1	1.4	1.8	1.7	3.5	1.4	1.5	1.6	1.4

655

656 **Extended Data Fig. 6: Monoclonal antibody ELISAs. a,** Graph shows antibody binding to
657 SARS-CoV-2 RBD. ELISA EC_{50} (half-maximal response) values for 84 antibodies isolated from
658 Moderna vaccinees measured at 8 weeks after the boost and from convalescent individuals at 1.3
659 and 6.2 months[6,7]. Horizontal bars indicate geometric mean. Statistical significance was
660 determined using the two-tailed Mann–Whitney U-test. Average of two or more experiments. **b-**
661 **k,** Graphs show ELISA titrations for antibodies all 84 antibodies against the indicated RBD
662 variants. n = 84 samples and isotype antibody as indicated in the figure. Low-binding antibodies
663 are indicated in colors. Data are representative of two independent experiments. **l,** Table shows a
664 heat map summary of EC_{50} values for binding to wild type RBD and the indicated mutants for 17
665 top neutralizing antibodies.
666

667 **Supplementary Tables**

668 **<u>Supplementary Table 1</u>: Individual vaccinee characteristics**

669

SI Table 1. Individual vaccinee characteristics

	Demographic characteristics				Vaccination details					Serological assays									
						# of	Time between (days)			S protein (AUC)			RBD (AUC)			Neutralization titer (reciprocal dilution)		Flow cytometry and antibody cloning	
Participant ID	Age (years)	Sex	Race §	Ethnicity	Vaccine platform	doses received	1st & 2nd dose	1st dose & blood draw	2nd dose & blood draw	IgG	IgM	IgA	IgG	IgM	IgA	NT50	NT90	B cell phenotyping and Ig sequencing	Monoclonal antibodies expressed
MOD1	51	Male	W	Hispanic	Moderna	2	28	74	46	26940	3563	2663	20704	2420	1850	746	88	Yes/Yes	Yes
MOD2	35	Male	W	Non-Hispanic	Moderna	2	34	62	28	25504	4164	1187	15479	3784	894	250	33	Yes/Yes	Yes
MOD3	32	Male	W	Non-Hispanic	Moderna	2	31	78	47	32594	6028	2460	24797	5827	1282	513	73	Yes/Yes	Yes
MOD4	63	Female	W	Hispanic	Moderna	2	28	63	35	40526	3097	2897	36772	2483	1257	3567	587	Yes/Yes	Yes
MOD6	41	Female	W	Non-Hispanic	Moderna	2	28	89	61	26504	3109	1362	17388	2810	717	178	21	Yes/Yes	No
MOD7	62	Male	A	Non-Hispanic	Moderna	2	35	84	49	34325	4967	1120	25025	3194	662	452	80	Yes/Yes	No
MOD8	69	Female	W	Non-Hispanic	Moderna	2	35	96	63	25449	1406	2342	19284	1495	958	290	56	Yes/Yes	No
MOD9	67	Female	W	Non-Hispanic	Moderna	2	29	119	90	37818	3078	4881	33456	2172	2728	543	99	Yes/Yes	No
PFZ10	41	Male	W	Non-Hispanic	Pfizer/BioNTech	2	19	103	84	23279	3520	892	15275	2952	590	138	20	Yes/Yes	No
MOD11	30	Male	W	Non-Hispanic	Moderna	2	28	63	35	35789	3850	2287	27896	3307	994	594	111	Yes/Yes	No
PFZ12	53	Female	W	Non-Hispanic	Pfizer/BioNTech	2	21	83	62	31885	3764	1702	24996	2116	963	948	154	Yes/Yes	No
MOD13	45	Male	W	Non-Hispanic	Moderna	2	28	110	82	13938	1776	708	7767	2683	589	97	10	Yes/No	No
MOD15	49	Male	W	Non-Hispanic	Moderna	2	26	90	64	20451	3553	1354	12557	2776	680	298	46	Yes/No	No
PFZ16	67	Female	W	Non-Hispanic	Pfizer/BioNTech	2	22	119	97	22220	718	731	12741	872	539	496	60	Yes/No	No
MOD17	29	Male	AA	Non-Hispanic	Moderna	2	31	62	31	30322	2816	3325	22258	2685	1985	961	220	Yes/No	No
MOD18	59	Female	W	Non-Hispanic	Moderna	2	30	127	97	18999	11442	751	12621	9797	576	141	28	Yes/No	No
C001	38	Female	W	Non-Hispanic	Pfizer/BioNTech	2	22	57	35	37288	1418	1802	32003	1848	705	1329	268	Yes/Yes	No
C002	41	Male	W	Non-Hispanic	Pfizer/BioNTech	2	21	100	79	17898	1348	695	10205	825	572	160	36	Yes/No	No
C003	41	Male	W	Non-Hispanic	Moderna	2	28	49	21	39139	20424	5451	36509	22772	3065	1946	501	Yes/Yes	No
C004	37	Male	W	Non-Hispanic	Pfizer/BioNTech	2	21	91	70	30773	858	1409	21052	1733	720	444	115	Yes/Yes	No

§ = White (W); African American (AA); Asian (A), American Indian or Alaska Native (AI/AN); Pacific Islander (PI); Multiple (M); unknown (N/A)
All serological parameters reported here are derived from plasma samples. Reported data are the mean of two independent experiments.

670

671 **<u>Supplementary Table 2</u>: Antibody sequences from vaccinees is provided as a separate Excel**

672 **file.**

673 **<u>Supplementary Table 3</u>: CDR3 alignment of highly identical clonal sequences.**

SI Table 3. CDR3 alignment of highly identical clonal sequences

	Heavy chain				Light chain		
	IGHV	IGHD	IGHJ	CDRH3	IGLV	IGLJ	CDRL3
MOD8	IGHV1-58*01	IGHD2-15*01	IGHJ3*02	**AAPYCSGGSCYDAFDI**	IGKV3-20*01	IGKJ1*01	**QQYGSSPWT**
	IGHV1-58*01	IGHD2-15*01	IGHJ3*02	.....	IGKV3-20*01	IGKJ1*01	.....
	IGHV1-58*01	IGHD2-15*01	IGHJ3*02	.....	IGKV3-20*01	IGKJ1*01	.....
C004	IGHV1-58*01	IGHD2-15*01	IGHJ3*02	.....N.V.H.G...	IGKV3-20*01	IGKJ1*01	...DR....
MOD3	IGHV1-58*01	IGHD2-8*01	IGHJ3*02	.....T...G.N.	IGKV3-20*01	IGKJ1*01	.....
PFZ10	IGHV4-31*03	IGHD4-23*01	IGHJ4*02	**ARDYGGNSNYFGY**	IGKV1-33*01	IGKJ4*01	**QQYNNLPLT**
	IGHV4-31*03	IGHD4-23*01	IGHJ4*02	.....A...D.	IGKV1-33*01	IGKJ4*01	...GY....
MOD11	IGHV4-31*03	IGHD4-23*01	IGHJ4*02	.....	IGKV1-33*01	IGKJ4*01	...D.....
	IGHV4-31*03	IGHD4-23*01	IGHJ4*02	...F.....D.	IGKV1-33*01	IGKJ4*01	...D.....
MOD8	IGHV4-31*03	IGHD4-23*01	IGHJ4*02	...F.....A.	IGKV1-33*01	IGKJ4*01	...D.....

674

675 **<u>Supplementary Table 4</u>: Sequences, half maximal effective concentrations (EC50s) and**

676 **inhibitory concentrations (IC50s) of the cloned monoclonal antibodies is provided as a**

677 **separate Excel file.**

678

679 **<u>Supplementary Table 5</u>: Neutralization activity of mAbs against mutant SARS-CoV-2**

680 **pseudoviruses.**

SI Table 5. Neutralization activity of mAbs against mutant SARS-CoV-2 pseudoviruses

	wt		R683G		R346S		K417N		N439K		N440K		Y453F		A475V		S477R		R683G/E484K		Q493R		N501Y		D614G	
	IC50 [ng/ml]	IC90 [ng/ml]	IC50 [ng/ml]	IC90 [ng/ml]	IC50 [ng/ml]	IC90 [ng/ml]	IC50 [ng/ml]	IC90 [ng/ml]	IC50 [ng/ml]	IC90 [ng/ml]	IC50 [ng/ml]	IC90 [ng/ml]	IC50 [ng/ml]	IC90 [ng/ml]	IC50 [ng/ml]	IC90 [ng/ml]	IC50 [ng/ml]	IC90 [ng/ml]	IC50 [ng/ml]	IC90 [ng/ml]	IC50 [ng/ml]	IC90 [ng/ml]	IC50 [ng/ml]	IC90 [ng/ml]	IC50 [ng/ml]	IC90 [ng/ml]
C601	2.0	9.2	1.4	6.3	1.9	11.5	1.4	6.4	1.8	8.5	2.2	10.2	1.2	7.9	1.8	11.9	1.9	8.3	112.2	630.3	2.6	13.5	4.9	13.8	2.5	8.5
C602	13.5	170.2	10.3	142.3	7.8	75.8	4.8	37.0	15.8	224.3	16.3	185.2	13.1	210.4	11.2	111.9	13.5	116.3	>1000	>1000	57.6	>1000	82.4	684.6	9.9	70.6
C603	14.3	129.9	6.7	89.5	208.7	>1000	4.9	38.8	11.8	170.2	13.2	115.1	11.7	163.0	19.1	208.3	11.3	112.5	>1000	>1000	7.1	78.5	56.1	292.9	10.8	130.7
C613	20.4	127.1	16.4	93.8	12.4	97.7	273.1	>1000	45.3	224.7	22.3	119.4	46.7	311.3	>1000	>1000	32.9	261.2	30.0	105.7	236.3	>1000	>1000	>1000	13.3	105.0
C614	5.0	20.2	3.7	16.9	4.1	26.7	>1000	>1000	3.9	20.7	5.7	23.1	4.7	34.6	31.7	215.3	4.4	20.2	9.4	26.6	6.6	41.5	16.1	37.1	4.2	17.6
C627	4.8	39.3	2.5	21.8	3.7	43.6	6.6	104.1	3.4	25.7	4.5	35.6	4.2	46.7	3.9	43.6	2.7	16.3	>1000	>1000	>1000	>1000	18.3	75.2	4.2	22.5
C628	18.8	169.9	11.6	144.3	8.6	95.3	5.2	63.4	257.3	>1000	29.8	216.2	36.5	570.6	16.1	120.1	17.9	147.2	>1000	>1000	146.8	>1000	>1000	>1000	13.6	98.4
C643	1.5	9.9	0.9	3.6	1.4	10.5	1.5	6.6	1.8	12.6	2.0	10.4	0.7	5.2	1.6	9.9	1.8	7.2	>1000	>1000	1.3	10.9	6.3	14.5	2.5	10.6
C653	9.7	45.7	7.4	42.4	6.6	47.5	>1000	>1000	7.7	36.0	9.3	43.0	18.7	109.8	20.0	126.2	10.0	41.1	>1000	>1000	168.3	875.2	34.3	100.7	8.4	39.9
C660	5.8	35.4	4.4	25.8	5.1	46.1	412.7	>1000	8.7	40.6	7.8	31.4	5.2	38.2	7.5	39.0	5.0	28.8	10.7	27.1	8.2	47.7	16.7	44.4	5.2	24.5
C663	11.5	103.7	8.5	90.6	7.6	91.7	79.6	>1000	18.9	222.4	14.4	91.7	14.4	158.5	382.1	>1000	16.5	154.1	31.7	143.3	60.2	922.1	>1000	>1000	11.5	117.8
C666	3.7	19.2	2.3	11.7	3.6	20.6	2.1	10.5	3.0	14.7	4.0	19.5	2.8	17.0	6.7	72.9	3.4	13.2	239.8	901.3	4.2	32.8	10.0	29.7	3.7	13.6
C669	15.5	183.0	17.5	164.1	9.4	169.1	12.0	96.1	>1000	>1000	>1000	>1000	20.4	154.0	13.3	172.5	13.5	146.3	24.1	258.5	13.1	177.3	141.0	469.8	16.7	84.6
C670	13.8	168.9	12.1	125.2	10.1	148.8	7.6	73.7	>1000	>1000	15.9	87.7	16.6	219.6	12.4	129.6	10.8	156.0	50.4	246.3	15.4	296.2	>1000	>1000	13.2	85.1
C671	5.4	37.8	3.1	22.7	5.9	47.1	4.5	29.2	4.8	33.1	6.9	35.3	5.6	38.8	5.9	42.3	4.7	34.5	>1000	>1000	282.8	>1000	27.7	84.4	5.1	24.3
C675	19.5	111.6	12.3	92.9	15.0	129.3	11.3	76.8	17.2	78.9	22.7	105.5	18.1	140.4	38.3	225.3	15.0	91.5	23.9	78.1	13.7	110.8	71.3	190.9	13.3	82.3
C682	45.3	196.0	29.4	191.9	25.9	199.6	>1000	>1000	23.3	132.0	43.2	215.0	12.4	85.3	>1000	>1000	62.3	367.1	110.4	478.6	214.3	>1000	383.2	>1000	28.0	232.8

Supplementary Table 6: Cryo-EM data collection and processing statistics

Table S6. Cryo-EM data collection and processing statistics

	C601 Fab SARS-CoV-2 S 6P	C603 Fab SARS-CoV-2 S 6P	C643 Fab SARS-CoV-2 S 6P	C663 Fab SARS-CoV-2 S 6P	C666 Fab SARS-CoV-2 S 6P	C669 Fab SARS-CoV-2 S 6P	C670 Fab SARS-CoV-2 S 6P
EMD	**xxxx**	**xxxx**	**xxxx**	**xxxx**	**xxxx**	**xxxx**	**xxxx**
Data collection conditions							
Microscope	Talos Arctica	Talos Artica	Talos Artica	Talos Artica	Talos Arctica	Talos Artica	Talos Artica
Camera	Gatan K3 Summit	Gatan K3 Summit	Gatan K3 Summit	Gatan K3 Summit	Gatan K3 Summit	Gatan K3 Summit	Gatan K3 Summit
Magnification	45,000x	45,000x	45,000x	45,000x	45,000x	45,000x	45,000x
Voltage (kV)	200	200	200	200	200	200	200
Recording mode	counting	counting	counting	counting	counting	counting	counting
Dose rate (e /pixel/s)	13.5	13.5	13.8	13.3	13.5	13.8	13.3
Electron dose (e /Å^2)	60	60	60	60	60	60	60
Defocus range (μm)	0.7 – 2.0	0.7 – 2.0	0.7 – 2.0	0.7 – 2.0	0.7 – 2.0	0.7 – 2.0	0.7 – 2.0
Pixel size (Å)	0.8689	0.8689	0.8689	0.8689	0.8689	0.8689	0.8689
Micrographs collected	846	1,053	1,849	1,200	2,059	1,961	1,863
Micrographs used	796	1,053	1,487	1,005	1,975	1,720	1,863
Total extracted particles	187,627	490,663	340,563	268,485	256,500	265,364	596,506
Refined particles	101,271	57,573	117,987	108,407	127,936	129,917	140,171
Particles in final refinement	37,665	57,573	54,392	48,088	42,582	54,129	140,171
Symmetry imposed	C1	C1	C1	C1	C1	C1	C1
FSC=0.143 Resolution (Å)	6.5	6.4	5.0	8.3	5.1	4.9	6.9

686 **References**

687 1 Gaebler, C. & Nussenzweig, M. C. All eyes on a hurdle race for a SARS-CoV-2 vaccine.
688 *Nature* **586**, 501-502, doi:10.1038/d41586-020-02926-w (2020).
689 2 Krammer, F. SARS-CoV-2 vaccines in development. *Nature* **586**, 516-527,
690 doi:10.1038/s41586-020-2798-3 (2020).
691 3 Jackson, L. A. *et al.* An mRNA Vaccine against SARS-CoV-2 - Preliminary Report. *N*
692 *Engl J Med* **383**, 1920-1931, doi:10.1056/NEJMoa2022483 (2020).
693 4 Polack, F. P. *et al.* Safety and Efficacy of the BNT162b2 mRNA Covid-19 Vaccine. *N*
694 *Engl J Med* **383**, 2603-2615, doi:10.1056/NEJMoa2034577 (2020).
695 5 Walsh, E. E. *et al.* Safety and Immunogenicity of Two RNA-Based Covid-19 Vaccine
696 Candidates. *N Engl J Med* **383**, 2439-2450, doi:10.1056/NEJMoa2027906 (2020).
697 6 Gaebler, C. *et al.* Evolution of Antibody Immunity to SARS-CoV-2. *bioRxiv*,
698 doi:10.1101/2020.11.03.367391 (2020).
699 7 Robbiani, D. F. *et al.* Convergent antibody responses to SARS-CoV-2 in convalescent
700 individuals. *Nature* **584**, 437-442, doi:10.1038/s41586-020-2456-9 (2020).
701 8 Schmidt, F. *et al.* Measuring SARS-CoV-2 neutralizing antibody activity using
702 pseudotyped and chimeric viruses. *J Exp Med* **217**, doi:10.1084/jem.20201181 (2020).
703 9 Widge, A. T. *et al.* Durability of Responses after SARS-CoV-2 mRNA-1273
704 Vaccination. *N Engl J Med* **384**, 80-82, doi:10.1056/NEJMc2032195 (2021).
705 10 Weisblum, Y. *et al.* Escape from neutralizing antibodies by SARS-CoV-2 spike protein
706 variants. *Elife* **9**, doi:10.7554/eLife.61312 (2020).
707 11 Baum, A. *et al.* Antibody cocktail to SARS-CoV-2 spike protein prevents rapid
708 mutational escape seen with individual antibodies. *Science* **369**, 1014-1018,
709 doi:10.1126/science.abd0831 (2020).
710 12 Davies, N. G. *et al.* Estimated transmissibility and severity of novel SARS-CoV-2
711 Variant of Concern 202012/01 in England. *medRxiv*, 2020.2012.2024.20248822,
712 doi:10.1101/2020.12.24.20248822 (2020).
713 13 Greaney, A. J. *et al.* Comprehensive mapping of mutations to the SARS-CoV-2 receptor-
714 binding domain that affect recognition by polyclonal human serum antibodies. **588**, 682-
715 635, doi:10.1101/2020.12.31.425021 (2021).
716 14 Greaney, A. J. *et al.* Complete Mapping of Mutations to the SARS-CoV-2 Spike
717 Receptor-Binding Domain that Escape Antibody Recognition. *Cell Host Microbe* **29**, 44-
718 57 e49, doi:10.1016/j.chom.2020.11.007 (2021).
719 15 Japan, N. I. o. I. D. Brief report: New Variant Strain of SARS-CoV-2 Identified in
720 Travelers from Brazil. doi:https://www.niid.go.jp/niid/images/epi/corona/covid19-33-en-
721 210112.pdf (2021).
722 16 Lauring, A. S. & Hodcroft, E. B. Genetic Variants of SARS-CoV-2-What Do They
723 Mean? *JAMA*, doi:10.1001/jama.2020.27124 (2021).
724 17 Tegally, H. *et al.* Emergence and rapid spread of a new severe acute respiratory
725 syndrome-related coronavirus 2 (SARS-CoV-2) lineage with multiple spike mutations in
726 South Africa. *medRxiv*, 2020.2012.2021.20248640, doi:10.1101/2020.12.21.20248640
727 (2020).
728 18 Briney, B., Inderbitzin, A., Joyce, C. & Burton, D. R. Commonality despite exceptional
729 diversity in the baseline human antibody repertoire. *Nature* **566**, 393-397,
730 doi:10.1038/s41586-019-0879-y (2019).

19 Andreano, E. *et al.* SARS-CoV-2 escape in vitro from a highly neutralizing COVID-19 convalescent plasma. *bioRxiv* **5**, 237-236, doi:10.1101/2020.12.28.424451 (2020).
20 Barnes, C. O. *et al.* SARS-CoV-2 neutralizing antibody structures inform therapeutic strategies. *Nature* **588**, 682-687, doi:10.1038/s41586-020-2852-1 (2020).
21 Barnes, C. O. *et al.* Structures of Human Antibodies Bound to SARS-CoV-2 Spike Reveal Common Epitopes and Recurrent Features of Antibodies. *Cell* **182**, 828-842 e816, doi:10.1016/j.cell.2020.06.025 (2020).
22 Thomson, E. C. *et al.* The circulating SARS-CoV-2 spike variant N439K maintains fitness while evading antibody-mediated immunity. *bioRxiv*, 2020.2011.2004.355842, doi:10.1101/2020.11.04.355842 (2020).
23 Tortorici, M. A. *et al.* Ultrapotent human antibodies protect against SARS-CoV-2 challenge via multiple mechanisms. *Science* **370**, 950-957, doi:10.1126/science.abe3354 (2020).
24 Starr, T. N. *et al.* Prospective mapping of viral mutations that escape antibodies used to treat COVID-19. *bioRxiv*, 2020.2011.2030.405472, doi:10.1101/2020.11.30.405472 (2020).
25 Lauring, A. S. & Hodcroft, E. B. Genetic Variants of SARS-CoV-2-What Do They Mean? *JAMA*, 1-3, doi:10.1001/jama.2020.27124 (2021).
26 Singer, J., Gifford, R., Cotten, M. & Robertson, D. CoV-GLUE: A Web Application for Tracking SARS-CoV-2 Genomic Variation. *Preprints*, doi:10.20944/preprints202006.0225.v1 (2020).
27 Elbe, S. & Buckland-Merrett, G. Data, disease and diplomacy: GISAID's innovative contribution to global health. *Glob Chall* **1**, 33-46, doi:10.1002/gch2.1018 (2017).
28 Voloch, C. M. *et al.* Genomic characterization of a novel SARS-CoV-2 lineage from Rio de Janeiro, Brazil. *medRxiv* (2020).
29 Hsieh, C. L. *et al.* Structure-based design of prefusion-stabilized SARS-CoV-2 spikes. *Science* **369**, 1501-1505, doi:10.1126/science.abd0826 (2020).
30 Brouwer, P. J. M. *et al.* Potent neutralizing antibodies from COVID-19 patients define multiple targets of vulnerability. *Science* **369**, 643-650, doi:10.1126/science.abc5902 (2020).
31 Cao, Y. *et al.* Potent Neutralizing Antibodies against SARS-CoV-2 Identified by High-Throughput Single-Cell Sequencing of Convalescent Patients' B Cells. *Cell* **182**, 73-84 e16, doi:10.1016/j.cell.2020.05.025 (2020).
32 Ju, B. *et al.* Human neutralizing antibodies elicited by SARS-CoV-2 infection. *Nature* **584**, 115-119, doi:10.1038/s41586-020-2380-z (2020).
33 Liu, L. *et al.* Potent neutralizing antibodies against multiple epitopes on SARS-CoV-2 spike. *Nature* **584**, 450-456, doi:10.1038/s41586-020-2571-7 (2020).
34 Rogers, T. F. *et al.* Isolation of potent SARS-CoV-2 neutralizing antibodies and protection from disease in a small animal model. *Science* **369**, 956-963, doi:10.1126/science.abc7520 (2020).
35 Zost, S. J. *et al.* Potently neutralizing and protective human antibodies against SARS-CoV-2. *Nature* **584**, 443-449, doi:10.1038/s41586-020-2548-6 (2020).
36 Schafer, A. *et al.* Antibody potency, effector function, and combinations in protection and therapy for SARS-CoV-2 infection in vivo. *J Exp Med* **218**, doi:10.1084/jem.20201993 (2021).

776 37 Mendoza, P. *et al.* Combination therapy with anti-HIV-1 antibodies maintains viral
777 suppression. *Nature* **561**, 479-484, doi:10.1038/s41586-018-0531-2 (2018).
778 38 Bar-On, Y. *et al.* Safety and antiviral activity of combination HIV-1 broadly neutralizing
779 antibodies in viremic individuals. *Nat Med* **24**, 1701-1707, doi:10.1038/s41591-018-
780 0186-4 (2018).
781 39 Li, Q. *et al.* The Impact of Mutations in SARS-CoV-2 Spike on Viral Infectivity and
782 Antigenicity. *Cell* **182**, 1284-1294 e1289, doi:10.1016/j.cell.2020.07.012 (2020).
783 40 Eguia, R. *et al.* A human coronavirus evolves antigenically to escape antibody immunity.
784 *bioRxiv* **5**, 52-28, doi:10.1101/2020.12.17.423313 (2020).
785 41 Amanat, F. *et al.* A serological assay to detect SARS-CoV-2 seroconversion in humans.
786 *Nat Med* **26**, 1033-1036, doi:10.1038/s41591-020-0913-5 (2020).
787 42 Grifoni, A. *et al.* Targets of T Cell Responses to SARS-CoV-2 Coronavirus in Humans
788 with COVID-19 Disease and Unexposed Individuals. *Cell* **181**, 1489-1501 e1415,
789 doi:10.1016/j.cell.2020.05.015 (2020).
790 43 Cohen, A. A. *et al.* Mosaic nanoparticles elicit cross-reactive immune responses to
791 zoonotic coronaviruses in mice. *Science*, doi:10.1126/science.abf6840 (2021).
792 44 Mastronarde, D. N. Automated electron microscope tomography using robust prediction
793 of specimen movements. *J Struct Biol* **152**, 36-51, doi:10.1016/j.jsb.2005.07.007 (2005).
794 45 Punjani, A., Rubinstein, J. L., Fleet, D. J. & Brubaker, M. A. cryoSPARC: algorithms for
795 rapid unsupervised cryo-EM structure determination. *Nat Methods* **14**, 290-296,
796 doi:10.1038/nmeth.4169 (2017).
797 46 Goddard, T. D. *et al.* UCSF ChimeraX: Meeting modern challenges in visualization and
798 analysis. *Protein Sci* **27**, 14-25, doi:10.1002/pro.3235 (2018).
799 47 Terwilliger, T. C., Adams, P. D., Afonine, P. V. & Sobolev, O. V. A fully automatic
800 method yielding initial models from high-resolution cryo-electron microscopy maps. *Nat*
801 *Methods* **15**, 905-908, doi:10.1038/s41592-018-0173-1 (2018).
802 48 Emsley, P., Lohkamp, B., Scott, W. G. & Cowtan, K. Features and development of Coot.
803 *Acta Crystallogr D Biol Crystallogr* **66**, 486-501, doi:10.1107/S0907444910007493
804 (2010).
805 49 Gupta, N. T. *et al.* Change-O: a toolkit for analyzing large-scale B cell immunoglobulin
806 repertoire sequencing data. *Bioinformatics* **31**, 3356-3358,
807 doi:10.1093/bioinformatics/btv359 (2015).
808 50 Soto, C. *et al.* High frequency of shared clonotypes in human B cell receptor repertoires.
809 *Nature* **566**, 398-402, doi:10.1038/s41586-019-0934-8 (2019).
810 51 Guo, Y., Chen, K., Kwong, P. D., Shapiro, L. & Sheng, Z. cAb-Rep: A Database of
811 Curated Antibody Repertoires for Exploring Antibody Diversity and Predicting Antibody
812 Prevalence. *Front Immunol* **10**, 2365, doi:10.3389/fimmu.2019.02365 (2019).
813 52 Kyte, J. & Doolittle, R. F. A simple method for displaying the hydropathic character of a
814 protein. *J Mol Biol* **157**, 105-132, doi:10.1016/0022-2836(82)90515-0 (1982).
815 53 Guy, H. R. Amino acid side-chain partition energies and distribution of residues in
816 soluble proteins. *Biophys J* **47**, 61-70, doi:10.1016/S0006-3495(85)83877-7 (1985).
817 54 DeWitt, W. S. *et al.* A Public Database of Memory and Naive B-Cell Receptor
818 Sequences. *PLoS One* **11**, e0160853, doi:10.1371/journal.pone.0160853 (2016).
819 55 Rubelt, F. *et al.* Onset of immune senescence defined by unbiased pyrosequencing of
820 human immunoglobulin mRNA repertoires. *PLoS One* **7**, e49774,
821 doi:10.1371/journal.pone.0049774 (2012).

822